

News from the Swampland – Constraining string theory with astrophysics and cosmology

Nils Schöneberg,¹ Léo Vacher,² J. D. F. Dias,^{3,4,5} Martim M. C. D. Carvalho,^{3,4} C. J. A. P. Martins^{3,5}

¹Institut de Ciències del Cosmos, Universitat de Barcelona, Martí i Franquès 1, Barcelona 08028, Spain

²Institut de Recherche en Astrophysique et Planétologie, CNRS/CNES, 9 avenue du Colonel Roche BP, Toulouse, France

²Université de Toulouse UPS, 118 route de Narbonne, Toulouse, France

³Centro de Astrofísica da Universidade do Porto, Rua das Estrelas 4150-762 Porto, Portugal

⁴Faculdade de Ciências, Universidade do Porto, Rua Campo Alegre 4169-007, Porto, Portugal

⁵Instituto de Astrofísica e Ciências do Espaço, CAUP, Universidade do Porto, Rua das Estrelas, 4150-762, Porto, Portugal

E-mail: nils.science@gmail.com

Abstract. Our current best guess for a unified theory of gravitation and quantum field theory (string theory) generically predicts a set of requirements for a consistently quantized theory, the Swampland criteria. Refined versions of these criteria have recently been shown to be in mild tension with cosmological observations. We summarize the status of the current impact of and constraints on the Swampland conjectures from cosmology, and subject a variety of dark energy quintessence models to recently released cosmological datasets. We find that instead of tightening the tension, the new data allows for slightly more freedom in the Swampland criteria. We further demonstrate that if there is no theoretical argument made to prevent interactions of the moduli fields with the electromagnetic sector, a novel fine-tuning argument arises from the extremely tight current constraints on such interactions. Finally, we conclude with a cautionary tale on model-independent reconstructions of the Swampland criteria from expansion rate data.

Contents

1	Introduction	1
2	Theory	3
2.1	The Swampland	3
2.2	Single-field Quintessence	4
2.3	Coupling to electromagnetism	6
3	Methodology and data	7
3.1	Implementation of Quintessence models	7
3.2	Data	8
4	Results	9
4.1	Model-specific investigation	9
4.1.1	Exponential model	9
4.1.2	Cosine potential	13
4.1.3	Axionic Cosine potential	15
4.1.4	Inverse exponential	16
4.1.5	Double exponential	18
4.2	Fine-tuning arguments	20
4.3	A note on model-independent reconstructions	22
4.4	Forecast constraints	27
5	Conclusions	27

1 Introduction

In the search for the fundamental physics underlying our universe the prediction of additional dynamical scalar fields is ubiquitous. They appear to be necessary components for most unifying frameworks beyond our contemporary standard models of particle physics and gravity, such as string theory. The spectrum of possible scalar field theories viable at the classical level is extremely large. In string theory, the different choices of compactification schemes for the extra spatial dimensions of space-time give rise to a vast number of possible solutions ($\gtrsim 10^{755}$ [1]), each featuring different scalar degrees of freedom associated to the compactified metric: the moduli fields. It is therefore a critical matter to understand and classify these solutions. The so-called Swampland program aims to find criteria on which to distinguish viable theories, part of the so-called Landscape, from the unacceptable ones, which constitute the Swampland. These criteria are based on the possibility to consistently quantize the theory, and as such related to UV completeness [2], and have been confirmed even in exotic corners of the string theory space [3]. For a complete review see [4, 5], and for critical discussions about the validity of the Swampland criteria see [6–11].

Scalar fields also underpin much of cosmology (such as in inflation, late-time dark energy, or possibly early dark energy), arising as foundational Lagrangian building blocks in a multitude of extensions (and serving also as useful tools to approximate more complicated models). As such, it is fundamentally important to ask how they can be constructed in a consistent unified theory. Indeed, Swampland conjectures have been extensively confronted with inflation models, showing significant tensions and providing strong restrictions on the allowed parameter space of the simplest class of models: those involving a single field¹ [12–18]. However, hope is not lost for inflationary scenarios remaining valid even when Swampland criteria are imposed, as a large variety of proposals has been put forth to rescue the inflationary paradigm. We list a small excerpt of such proposals below:

- In the context of multi-field inflation see e.g. [19–24].
- In the context of warm inflation see e.g. [25–32].
- In the context of eternal inflation see e.g. [33–36].
- In the context of natural or Starobinsky inflation see e.g. [16, 37].
- In the context of other inflationary paradigms see e.g. [38–44].
- In the context of modified gravity theories, see e.g. [45–54].
- In the context of avoiding Swampland conjectures through other means, see e.g. [55, 56] for excited initial states, [57] for Lorentz violation, and [58] for a tunneling wavefunction.

See also [59] for a discussion of re-heating in the context of the Swampland conjectures. Given this vast space of reconciling inflation with the Swampland conjectures, it is only natural to ask what other parts of cosmology feature scalar fields and how they are impacted by the conjectures.

The widely accepted Λ CDM cosmological model is built on the presence of a cosmological constant Λ whose origin is not trivial to explain, especially as computations of the vacuum energy in the standard model typically result in expectations many orders of magnitude higher [60]. As such, in most high energy extensions of the standard model the cosmological constant is abandoned in favor of a dynamical dark energy. Moreover, in many realizations of string theory the dark energy – responsible for the late time acceleration of the universe – must necessarily be promoted to a dynamical field, subject to the same Swampland criteria. Indeed, due to the challenges of constructing a de Sitter vacuum in string theory, it is possible to motivate Swampland conjectures arguing that any such vacuum is not part of the Landscape. In turn this implies that – in a consistent theory of quantum gravity – dark energy must be dynamical at some level [61]. Therefore the Swampland conjectures can also be used to investigate the nature of dark energy. While our current Λ CDM model is built on the assumption that dark energy is sourced by a single cosmological constant, Λ , emerging from general relativity, it seems extremely difficult to build such a state from string theoretical considerations.

Quintessence provides the simplest form of dynamical dark energy in the form of a scalar field driving the late time acceleration of our universe’s expansion [62]. It is clear that if one accepts the Swampland conjectures, many of the arguments and constraints applying in the inflationary context will also apply here, and therefore the Swampland conjectures also allow to put stringent restrictions on the possibility for a scalar field to source dark energy. In the context of quintessence, the Swampland conjectures have been invoked in [6, 63–68], and in other late-time model-specific contexts in [69–75]. Instead, analyses of the implications of the Swampland conjectures have also been made for the low-redshift universe in a more model-independent way in [76–81]. The general conclusion of these works is a mild but not insurmountable tension between late time observations of dark energy and the Swampland criteria.

¹As we will see later, the de-Sitter Swampland criteria essentially requires the slow roll conditions to be explicitly broken, making single field inflation rather difficult to construct consistently.

In the present work we aim to give a compressed overview of the Swampland criteria in the context of cosmology, with a particular focus on its applications to late-time cosmology and single-field quintessence models. In particular, we are going to outline that the present tension persists in a weakened form with new data, both for model-specific and model-independent analyses. We are also going to present novel fine-tuning arguments about possible interactions of the quintessence fields with other standard model fields. These arguments show that if the interactions are not forbidden for some deeper physical reason, current local and astrophysical tests on the stability of the fine structure constant α are significantly more stringent than analogous constraints on dark energy, and therefore have a significant impact on the consequences of the conjectures.

In Section 2 we shortly review the theoretical foundations of the Swampland program with a special focus on the applicability to quintessence. We then present our methodology and data in Section 3, while our results will be shown in Section 4. We conclude in Section 5.

2 Theory

In this section we briefly review some theoretical foundations, and establish our notation. The interested reader is encouraged to look into the reviews cited below for more information beyond the succinct summary presented here. In Section 2.1 we summarize the state of the Swampland conjectures in terms of cosmology, and in Section 2.2 we briefly summarize the quintessence model and its relation to the Swampland conjectures.

2.1 The Swampland

Here we only provide a short succinct summary of the state of the Swampland program, for more details we refer the reader to [4–6].

At the present stage, the Swampland program consists of a set of conjectures, generally based on attempts to construct stable quantum theories of gravity. Typically, one encounters such conditions when seeking for viable vacuums of string theory, when making considerations regarding black holes, or when assessing the possibility to recover effective field theories emerging from underlying micro-physics [4].

Perhaps one of the most fundamental conjectures is the distance conjecture. In its fundamental form it simply states the necessity of an infinite tower of mass states (related to the expectation values of the underlying fields), which occurs somewhere at an infinite distance within the (non-compact) manifold spanned by the fields (the moduli space) [82]. However, this distance conjecture has been recently refined in [83, 84]. In its refined form, the conjecture argues that the infinite tower of light states already appears for trans-Planckian field variations and even in the case of moduli fields subject to a potential. Invoking an upper bound on the allowed number of light states² (such as the Bousso bound [85], which extends the Bekenstein bound on space-time entropy [86, 87], or alternatively arguments about the breakdown of the effective low-energy field theory [5]), one can convert this statement into the requirement that trans-Planckian excursions can not be allowed for any fields present in the cosmological evolution. We will refer to this specialized Swampland distance conjecture simply as the **distance conjecture**:

$$|\Delta\phi|/M_{\text{pl}} < \mathcal{O}(1) , \tag{2.1}$$

with M_{Pl} being the reduced Planck mass³, $M_{\text{Pl}}^{-2} = 8\pi G$. It should be kept in mind that there is a small degree of variation of the constraint in the values for many string theory realizations, so the exclusion of a unity-order value is not strictly a large problem.

²This is not as trivial as it might seem, as these mass states could not only be particles but also extended objects such as cosmic strings. We are going to remain agnostic and follow the literature in this regard, and formulate the conjecture as a restriction of the possible low-energy theory.

³We work in natural units ($c = \hbar = 1$).

Due to the difficulties of consistently constructing the meta-stable de-Sitter vacua at the heart of cosmology, [88]⁴ has further proposed a requirement on possible field potentials of theories in the Landscape, given by

$$\text{either } M_{\text{Pl}} \frac{|V'|}{V} \gtrsim \mathcal{O}(1) \quad \text{or} \quad -M_{\text{Pl}}^2 \frac{V''}{V} \gtrsim \mathcal{O}(1), \quad (2.2)$$

where a prime denotes the derivative with respect to the field. We are going to denote these two alternative de-Sitter constraints as the **first Swampland criterion** and **second Swampland criterion**, respectively. Note that a combined further refinement has been put forth in [89]. Finally, in order to simplify notation, we introduce

$$\lambda(z) = M_{\text{Pl}} |V'(z)/V(z)|, \quad \text{and} \quad g(z) = -M_{\text{Pl}}^2 V''(z)/V(z). \quad (2.3)$$

Any one of these two critical functions (of which we have made the redshift dependence explicit) needs to be positive and at least of order unity for the de-Sitter constraints to hold. There are also a few criteria beyond these most well-known ones, such as excellently summarized in [4], but we are not going to use those in the context of this work.

2.2 Single-field Quintessence

Quintessence is a framework in which dark energy is a dynamical degree of freedom, responsible for the accelerated expansion seen in recent cosmological history. It is a simple modification of Λ CDM, where the cosmological constant is replaced by one or more additional scalar fields minimally coupled to gravity as:

$$S = \int d^4x \sqrt{-g} \cdot \left\{ M_{\text{Pl}}^2 \frac{R}{2} - \frac{1}{2} g^{\mu\nu} G_{ij} \partial_\mu \phi^i \partial_\nu \phi^j - V(\phi) + \dots \right\}, \quad (2.4)$$

where G_{ij} is a metric over field space, which reduces to 1 in the single-field case, $g_{\mu\nu}$ is the usual metric and g its determinant. Assuming a single field, it is quite simple to find the Klein-Gordon equation of motion at the background level

$$\ddot{\phi} + 3H\dot{\phi} + V'(\phi) = 0, \quad (2.5)$$

and at the level of the field perturbation $\delta\phi$ with

$$\delta\ddot{\phi} + 3H\delta\dot{\phi} + \dot{h}\dot{\phi}/2 + [k^2/a^2 + V''(\phi)] \delta\phi = 0, \quad (2.6)$$

in the comoving synchronous gauge (for the Newtonian gauge, see [90, Eq. 4.3]). Here $V'(\phi)$ and $V''(\phi)$ denote the first and second derivatives of the potential $V(\phi)$ with respect to the field ϕ . The field density and pressure are given by

$$\rho_\phi = \frac{1}{2} \dot{\phi}^2 + V \quad \text{and} \quad P_\phi = \frac{1}{2} \dot{\phi}^2 - V. \quad (2.7)$$

These are also related by the trivial energy conservation $\dot{\rho}_\phi = -3H(\rho_\phi + P_\phi) = -3H\dot{\phi}^2$ that is directly equivalent to Eq. (2.5). If the field is dominated by the potential contribution its equation of state $w_\phi = P_\phi/\rho_\phi$ tends towards -1 , while in the kinetically dominated regime it tends towards $+1$.

For the Friedmann equation one can simply add the field energy density to the other densities:

$$H^2 = \frac{8\pi G}{3} \rho_{\text{tot}} = \frac{8\pi G}{3} \left[\rho_a + \frac{1}{2} \dot{\phi}^2 + V(\phi) \right], \quad (2.8)$$

where ρ_a denotes all other components contributing to the energy density (such as radiation, cold dark matter, baryons, neutrinos, ...). The energy conservation of the total content of the universe implies immediately that

$$\dot{\rho}_{\text{tot}} = -3H(\rho_{\text{tot}} + P_{\text{tot}}) = -3H\rho_{\text{tot}}(1 + w_{\text{eff}}), \quad (2.9)$$

⁴The first swampland criterion had already been proposed in for example [61], though the connection to the distance conjecture has been clarified in [88].

where $w_{\text{eff}} = P_{\text{tot}}/\rho_{\text{tot}} = (P_a + P_\phi)/(\rho_a + \rho_\phi) = r_a w_a + r_\phi w_\phi$, with $r_x = \rho_x/\rho_{\text{tot}}$ and $w_x = P_x/\rho_x$. In order to check what conditions the field must satisfy in order to be responsible for the universe's acceleration, we can differentiate the Friedmann equation with respect to time, substituting $\dot{\rho}_{\text{tot}}$ for Eq. (2.9) and divide by $2H$, obtaining the well known second Friedmann equation

$$\dot{H} = -\frac{3}{2}H^2(1 + w_{\text{eff}}), \quad (2.10)$$

which can be explicitly written to isolate the acceleration of the universe

$$\ddot{a} = -\frac{1}{2}aH^2(1 + 3w_{\text{eff}}). \quad (2.11)$$

Clearly, to allow for the accelerated expansion of the universe observed at late times, we need $w_{\text{eff}} < -1/3$ to achieve $\ddot{a} > 0$. This immediately allows us to put a constraint on the equation of state of the scalar field such that $w_\phi < (-1/3 - r_a w_a)/r_\phi$, with $r_a > 0$ and $w_a \approx 0$ at low redshift ($z < 5$), where the dark energy can become important. As such, we are left with approximately $w_\phi < -1/(3r_\phi)$, requiring at least a mild domination of the potential energy of the field with respect to the kinetic energy. The underlying problem of fulfilling the Swampland criteria in this regime is that a large $V'(\phi)$ will – through Eq. (2.5) – typically quickly accelerate the field and thus make it hard for the overall potential to dominate.

In order to analyze the dynamics of the quintessence model, it is often useful to reparameterize it through [91]

$$x = \frac{\dot{\phi}}{\sqrt{6}M_{\text{Pl}}H}, \quad y = \frac{\sqrt{V}}{\sqrt{3}M_{\text{Pl}}H}. \quad (2.12)$$

Using these variables, one simply has $\rho_\phi/(3M_{\text{Pl}}^2H^2) = \rho_\phi/\rho_{\text{tot}} = x^2 + y^2$, so iso-density contours represent a simple circular arc. The field and Friedmann equations then give rise to non-linear first-order differential equations for x and y

$$\frac{\partial x}{\partial \ln a} = -3x + \frac{\sqrt{6}}{2}L \cdot y^2 - x \frac{\partial \ln H}{\partial \ln a}, \quad (2.13)$$

$$\frac{\partial y}{\partial \ln a} = -\frac{\sqrt{6}}{2}L \cdot xy - y \frac{\partial \ln H}{\partial \ln a}. \quad (2.14)$$

$$(2.15)$$

where $L = -M_{\text{Pl}}V'/V$ (such that from Eq. (2.3) we have $\lambda(z) = |L|$). The flow of the trajectories in this (x, y) space can be analyzed using a dynamical system approach. We show the possible trajectories in Fig. 1 for a few values of L , with the red iso-density contour marking complete dark energy domination ($x^2 + y^2 = \rho_\phi/\rho_{\text{tot}} = 1$), and the yellow iso-density contour marking the observation of dark energy density in the late universe from supernovae data, at around ($x^2 + y^2 \simeq 0.7$). The two non-trivial fixed points are $(x, y) = (L/\sqrt{6}, \sqrt{1 - L^2/6})$ (red dot) and⁵ $(x, y) = (\sqrt{3/2}/L, \sqrt{3/2}/L)$ (blue dot). The red fixed point at $x^2 + y^2 = 1$ is the growing attractor solution as long as the blue solution does not reach the boundary, i.e. for $L \leq \sqrt{3} \simeq 1.73$. This means that for $L^2 > 3$ the universe cannot ever be fully dominated by dark energy, even in the infinite future. However, this is technically not even required by the current observations, which only set a weaker condition that the current amount of cosmic acceleration has to be explained by some dark energy, which gives the weaker condition of $x^2 + y^2 \simeq (1 - \Omega_m) \approx 0.7$. This condition can be fulfilled for even higher values of L . At the point where $L = \sqrt{3}$ the two non-trivial fixed points intersect at $(x, y) = (1/\sqrt{2}, 1/\sqrt{2})$, after which they exchange their attractive/repulsive behavior. The attractive point is now the blue one, which for a given L can reach up to $x^2 + y^2 = 3/L^2$. This means that for the aforementioned reason we instead have the weaker condition $L \lesssim 2.1$.

⁵The true fixed point is at $(x, y) = (\sqrt{3/2}/L \cdot (1 + w_a), \sqrt{3/2}/L \cdot \sqrt{1 - w_a^2})$. In order to simplify the discussion we explicitly set $w_a = 0$ (which is a very good approximation at the redshifts of interest). In the full parameter space the point approaches the $x^2 + y^2 = 1$ boundary only as $L^2 \rightarrow 3(1 + w_a)$, but otherwise the discussion remains the same.

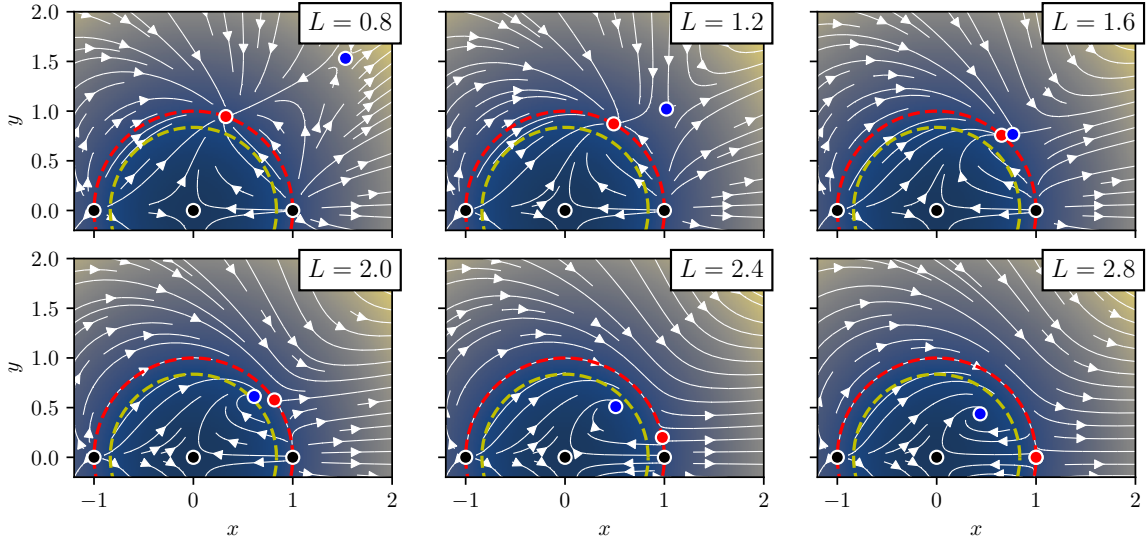


Figure 1. Differential equation flows in the (x, y) plane for various values of $L = -M_{\text{Pl}}V'/V$. The arrows show the directions of (\dot{x}, \dot{y}) . The red dashed line shows $x^2 + y^2 = 1$, while the yellow dashed line shows $x^2 + y^2 = 0.7$. The colored dots denote the critical points (where the gradient is zero). The trivial critical points at $y = 0$ are colored in black. For $L < \sqrt{3} \simeq 1.73$ the blue fixed point is repulsive and further from the origin than the red fixed point at $x^2 + y^2 = 1$. For $L > \sqrt{3}$ the blue point is closer to the origin and becomes attractive, while the red point becomes repulsive. Only as long as $L \lesssim \sqrt{3}/(1 - \Omega_m) \approx 2.1$ is the blue point at $x^2 + y^2 > 1 - \Omega_m$ (outside the yellow circle). At large $L > \sqrt{6} \simeq 2.45$ the red point joins the trivial critical point at $(x, y) = (1, 0)$.

Note that the system of Eqs. (2.13) and (2.14) obeys the symmetry $(x, y, L) \rightarrow (-x, -y, -L)$, so the condition can be rephrased equivalently as $\lambda(z) \lesssim 2.1$. This implies that the observed acceleration of the universe can only be realized as long as $\lambda(z) \lesssim 2.1$, whereas the first Swampland criterion requires $\lambda(z) \gtrsim \mathcal{O}(1)$. It is this inherent tension that makes the observed acceleration such a potent probe of the Swampland criteria.

The argument for the second Swampland criterion can be built upon the same basis, but is a bit more subtle. Here one can use

$$dL/d \ln a = \sqrt{6}M_{\text{Pl}} \cdot x \cdot (L^2 + g) , \quad (2.16)$$

where $g(z) = -M_{\text{Pl}}V''/V$ as in Eq. (2.3). If $g \gg 1$ we find that L is quickly accelerating, which is a self-sustaining process⁶ as evident from the equation. In this case the growing L will soon violate $\lambda(z) < 2.1$ required for the accelerating universe at the attractor.

Overall, we can summarize that the fulfillment of either Swampland criterion is in mild tension with the observation of an accelerating universe in the quintessence model. Exactly how strong this tension is will be investigated in Section 4, but even the simple analytical arguments performed here already demonstrate that the observation of the universe's expansion history can necessarily place tight constraints on the Swampland criteria.

2.3 Coupling to electromagnetism

In the most general setting, one expects new scalar fields ϕ present in the theory to be coupled to all the sectors of the standard model, unless some symmetry principle prevents this. There is no strong reason a priori why a UV-complete theory formulated within string theory should decouple such scalar

⁶Of course it is only self-sustaining since $g > 0$ in this case. In the exponential potential case, for example, we have $g = -L^2 < 0$, thus giving $dL/d \ln a = 0$ as expected.

fields from other fields in the low-energy limit applicable to most of cosmology. This, in turn, causes a major fine-tuning issue for the coupling parameter in order to remain consistent with observations (the impact of which is detailed in Section 4.2).

In practice, the most stringent bounds on such interactions are expected from the tightly constrained and well observed electromagnetic sector. We thus focus on a coupling of the field ϕ to the electromagnetic field curvature tensor of the form

$$\mathcal{L}_{\text{EM}} = -\frac{1}{4}B_F(\phi)F_{\mu\nu}F^{\mu\nu} , \quad (2.17)$$

as a Lagrangian addition to the full action of Eq. (2.4). Such a term naturally preserves the $U(1)$ gauge symmetry of the theory, and has been adopted in the past in the context of the Bekenstein model [92, 93] (we explored such coupled models in detail in [94], using a similar methodology as the present paper). In such a framework, the fine structure constant $\alpha = e^2/4\pi$ is not a constant anymore, and varies with the field as $\alpha(z)/\alpha(z=0) \propto B_F(\phi(z))^{-1}$. As no significant variation of α can be observed on cosmological scales, it is common to Taylor-expand the coupling at first order as

$$B_F(\phi) \simeq 1 + \zeta \cdot (\phi - \phi_0) , \quad (2.18)$$

with $\phi_0 = \phi(z=0)$ and $\zeta = \partial_\phi B_F(\phi)|_{\phi=\phi_0}$, using the sign convention of [93]. We confirm that since in our runs the field typically does not have large trans-Planckian movement this approximation remains valid. From here we can directly obtain the variation of the fine-structure constant as

$$\frac{\alpha(z) - \alpha(z=0)}{\alpha(z=0)} \simeq -\zeta \cdot [\phi(z) - \phi_0] . \quad (2.19)$$

In our investigation we will simply define $\alpha(z=0) = \alpha_0$, where $\alpha_0 \simeq 1/137$ is the value measured in earth-based laboratories [95]. Furthermore, taking the derivative of Eq. (2.19) with respect to $\ln a$, one finds the time variation of the fine structure constant

$$\frac{1}{\alpha_0} \frac{d\alpha}{d \ln a} = -\zeta \frac{d\phi}{d \ln a} , \quad (2.20)$$

which can be directly measured in laboratory with high accuracy.

3 Methodology and data

3.1 Implementation of Quintessence models

We implement the quintessence model in the Einstein-Boltzmann solver CLASS⁷[96]. We make use of the existing `scf` implementation by introducing a new component `cqf` (coupled quintessence field) with essentially the same equations of motion (which are those of Eqs. (2.5) and (2.6)). The main differences with respect to the `scf` implementation are the different underlying potentials, the initialization of the field, the ability to allow for additional coupling to electromagnetism, and some minor details on the parameter shooting. We list the potentials that we implemented and investigate in Section 4. The code is adapting in each case the amplitude of the potential in order to find a solution where the quintessence field makes up a given amount of dark energy ($1 - \Omega_m$) in order to achieve a flat universe (as favored from observations and inflationary theories).

The initialization of the field is always performed by providing ϕ_{ini} and $\dot{\phi}_{\text{ini}}$ at the initial time at which the CLASS background module begins computation. For all investigated cases we explicitly set $\dot{\phi}_{\text{ini}} = 0$ as a 'natural' initial condition. We vary ϕ_{ini} freely except where explicitly stated otherwise. Investigations with non-zero field speed initial conditions are left for future work.

⁷https://github.com/lesgourg/class_public

The additional coupling to electromagnetism is implemented using Eq. (2.19), where we assume for simplicity a constant coupling ζ . The time-variations of the fine structure constant $\alpha(z)$ are then self-consistently propagated to all parts of the code, such as for example during recombination (building on our previous analysis in [94, 97, 98] and made publicly available in the CLASS software), and are used as an output when combining with the data on $\alpha(z)$ or $\dot{\alpha}(z)$ that is described below.

We confront our quintessence models to data by running Monte Carlo Markov chains (MCMC) using the MONTEPYTHON⁸ software that is integrated with CLASS. Contour plots are made using GETDIST⁹. All chains have a Gelman-Rubin convergence criterion of $|R - 1| < 0.05$.

3.2 Data

The data we employ for our investigation of the cosmological constraints on the Swampland criteria are detailed below:

- **Planck:** The temperature and polarization CMB angular power spectra from the Planck 2018 satellite data release, using the Planck legacy likelihood¹⁰ [99], as well as the Planck lensing reconstruction [100].
- **BAO:** The baryonic acoustic oscillation (BAO) measurements of the angular diameter distance to the sound horizon standard ruler. This combination consists of the old DR12 BAO employed in [99], namely the 6dFGS [101] at $z = 0.1$, the MGS [102] at $z = 0.15$, and the DR12 LRGs [103] at $z = 0.38, 0.51, 0.61$.
- **BAO DR16:** The newly released measurements of the BAO from SDSS DR16 [104], namely in LRGs (luminous red galaxies) [105, 106] at $z = 0.38, 0.51, 0.7$, in QSOs (quasi-stellar-objects) [107, 108] at $z = 1.48$, in the Lyman- α forest at $z = 2.3$, and their correlation [109].
- **Pantheon:** The Pantheon supernova sample analysis from [110] containing 1048 supernovae up to $z < 2.3$. These standard candles effectively give a measurement of the expansion rate at low redshift.
- **PantheonPLUS:** The updated Pantheon supernova sample analysis from [111] containing 1550 supernovae also up to $z < 2.3$.
- **CC:** Cosmic chronometer data from [112], which are measurements of differential ages of galaxies to determine $H(z) \approx -\Delta z / [(1+z)\Delta t]$. We take into account systematic uncertainties outlined in [112] such as from the modeling of the star formation history.
- **ACT+SPT:** The ground-based ACT and SPT data from [113, 114], which provide the most precise non-Planck CMB anisotropy data to date.
- **QSO** (quasi-stellar-objects) We use spectroscopic measurements of quasars, allowing to recover the value of the fine structure constant α at different redshifts from Eq. (2.19). Our dataset – detailed in [94, 115] – contains more than 300 measurements obtained by the VLT-UVES and Keck-HIRES instruments, as well as points obtained from the HARPS, Subaru and ESPRESSO spectrograph, spanning a redshift range of $0.22 \leq z \leq 4.18$ [116–118].
- **Oklo** is a natural nuclear reactor which was active on Earth several billion years ago. From its abundances, one can obtain a bound of¹¹ $\Delta\alpha/\alpha = (0.005 \pm 0.061) \times 10^{-6}$ on the fine structure constant value of Eq. (2.19) at a redshift of $z = 0.14$ [119].

⁸https://github.com/brinckmann/montepython_public

⁹<https://getdist.readthedocs.io/en/latest/>

¹⁰<https://pla.esac.esa.int/>

¹¹This value is obtained from nuclear physics considerations which in turn are very model dependent; specifically, this bound is obtained on the assumption that α is the only dimensionless coupling whose value might not be the standard one. However, as we find later, this is not critical for our study as the final Oklo impact on ζ is of the same order of magnitude than the QSO data.

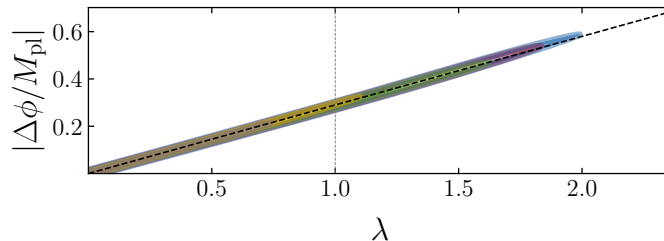


Figure 2. Correlation between the two Swampland criteria in the exponential case

- **AC** (atomic-clocks) By comparing the transition lines of different atoms in a laboratory, it is possible to obtain the highly restrictive limit on the drift rate of α from Eq. (2.20) of $d \ln \alpha / d \ln a = (2.5 \pm 3.5) \times 10^{-9}$ at $z = 0$ [120].

All the bounds related to the fine structure constant (QSO, Oklo and AC) are implemented as Gaussian prior likelihoods. We also combine the data from Planck, ACT, SPT, CC, BAO DR16 and PantheonPLUS into a data set \mathcal{A} (all). In order to test the impact of new and old data, we also create the dataset \mathcal{A}_{old} where we replace BAO DR16 with BAO, and PantheonPLUS with Pantheon.

4 Results

In this section we present the results of our investigations into the effect of the Swampland criteria Eqs. (2.1) and (2.2) on late-time cosmology and in regard to fine-tuning arguments for the coupling. We start the discussion by presenting constraints for specific models in Section 4.1, continue in Section 4.2 with a discussion of the extreme fine-tuning required for the coupling of a quintessence field with electromagnetism expected generically, and finish our discussion in Section 4.3 with a model-independent analysis of quintessence in the context of Swampland conjectures and a word of caution in regard to this analysis. We use the notation of $\lambda(z)$ and $g(z)$ from Eq. (2.3).

4.1 Model-specific investigation

To start our investigation on the coupled quintessence field in the context of the Swampland conjecture, we first revisit some of the commonly considered models. We show the latest constraints on the various models, and note a particularly interesting feature comparing old and new BAO and supernova data.

4.1.1 Exponential model

Perhaps the most interesting potential is the simple exponential model with

$$V(\phi) = A \exp(\lambda\phi/M_{\text{Pl}}) . \quad (4.1)$$

Here λ is a constant, and we do indeed have $\lambda(z) \equiv M_{\text{Pl}}|V'/V| = \lambda$. The exponential case is thus a case where the first Swampland criterion is taken to be constant. This can be argued to be the most conservative choice [66] when considering primarily the first Swampland criterion, as any other potential also includes regions with smaller $\lambda(z)$. The second Swampland criterion has $V''/V = \lambda^2$ implying $g(z) = -\lambda^2 < 0$, which can obviously never be positive, and is thus always violated. It also has an interesting relation to the distance criterion, which is shown in Fig. 2 and has been derived analytically in [66]. This relation is

$$|\Delta\phi/M_{\text{Pl}}| \approx \frac{\lambda}{3} \left[\frac{1}{\sqrt{1-\Omega_m}} \ln \left(\frac{1+\sqrt{1-\Omega_m}}{1-\sqrt{1-\Omega_m}} \right) - 2 \right] \approx 0.29\lambda , \quad (4.2)$$

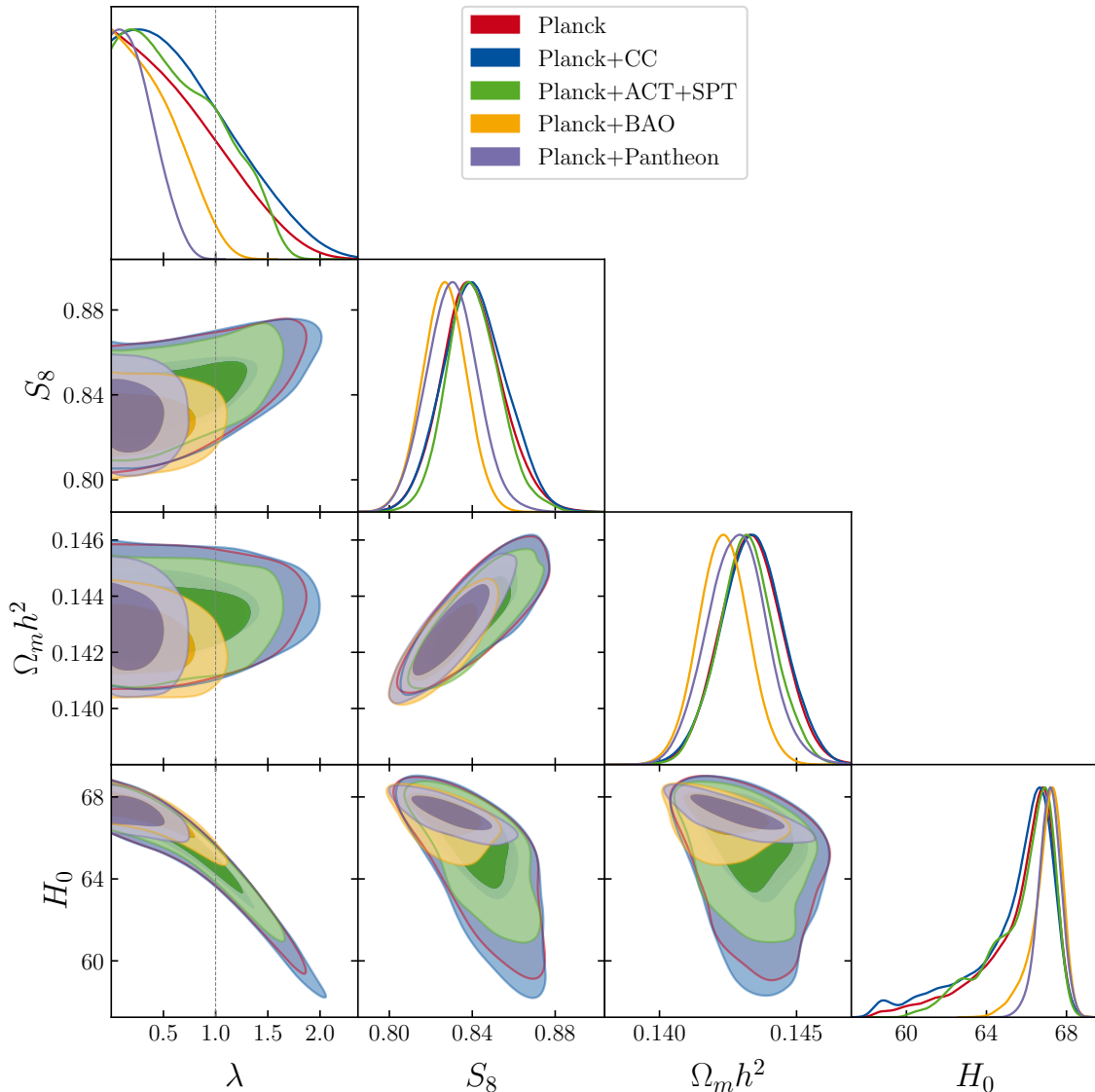


Figure 3. Comparison of the constraints on the exponential model for a variety of data sets.

where we used $\Omega_m \approx 0.31$. It is a result of the field being frozen due to Hubble drag during most of the history and only beginning to move when dark energy begins to dominate. Though, since this time-frame is relatively short, the overall displacement of the field is closely related to the slope of the potential during dark energy domination. This mapping immediately allows us to conclude that we primarily have to investigate the first Swampland criterion for this model, since the distance criterion will always be more easily satisfied than the first Swampland criterion, and the second Swampland criterion is by definition violated. As a final note, since we can always absorb a constant offset of $\phi \rightarrow \phi + p$ into a redefinition of the field amplitude $A \rightarrow A \exp(-\lambda p/M_{\text{Pl}})$ we can fix the initial condition to $\phi_{\text{ini}} = 0$.

We subject the exponential model to a variety of data in Fig. 3, showing precisely which cosmological probes give a tight constraint on the model and which do not. We also summarize the most interesting constraints in Table 1. We observe that while cosmic chronometer data in principle

Data combination	H_0 [km/s/Mpc]	λ (95% CL)	$P(\lambda > 1)$ in %	$P(\lambda > 0.1)$ in %
Planck	$65.6^{+1.6}_{-1.9}$	< 1.6	24	91
Planck +CC	$65.3^{+1.8}_{-2.2}$	< 1.7	28	93
Planck +ACT+SPT	$65.8^{+1.5}_{-1.7}$	< 1.4	24	91
Planck +BAO	67.02 ± 0.72	< 0.94	2.9	85
Planck +Pantheon	67.15 ± 0.56	< 0.62	< 0.001	79

Table 1. Constraints on H_0 and λ in the exponential coupled quintessence field model. We also cite the probability to exceed $\lambda > 1$.

Data combination	H_0 [km/s/Mpc]	λ (95% CL)	$P(\lambda > 1)$ in %	$P(\lambda > 0.1)$ in %
Planck +BAO	67.02 ± 0.72	< 0.94	2.9	85
Planck +BAO DR16	65.7 ± 1.2	< 1.3	23	94
Planck +Pantheon	67.15 ± 0.56	< 0.62	< 0.001	79
Planck +PantheonPLUS	66.59 ± 0.62	< 0.80	0.24	89

Table 2. Same as Table 1 for old and new BAO and Pantheon data.

Data combination	H_0 [km/s/Mpc]	λ (95% CL)	$P(\lambda > 1)$ in %	$P(\lambda > 0.1)$ in %
\mathcal{A}	$66.36^{+0.56}_{-0.54}$	< 0.85	0.33	0.93
$\mathcal{A} + H_0$	67.70 ± 0.50	< 0.60	< 0.001	0.80
\mathcal{A}_{old}	67.38 ± 0.40	< 0.60	< 0.001	0.77
$\mathcal{A}_{\text{old}} + H_0$	67.84 ± 0.39	< 0.46	< 0.001	0.74

Table 3. Same as Table 1 for combinations involving the \mathcal{A} =Planck, BAO, Pantheon, CC, ACT, and SPT data combination, and also for added H_0 priors.

probe the background expansion history, they do not allow for a tight constraint on the field evolution that would be noticeable in a tightened constraint on λ . Instead, the results are equivalent (or even slightly worse due to finite MCMC convergence). Instead, ACT+SPT data slightly restrict the highest values of λ . Even more constraining are BAO data which probe the late evolution and the matter fraction Ω_m tightly, reducing also the probability of $\lambda > 1$ with these data to below 5%. The most constraining data here are the Pantheon supernovae, which allow for a constraint of $\lambda < 0.62$ (95% CL) when combined with Planck. The probability of reaching $\lambda > 1$ in this model is so low that from the more than 2 million sampled points none have $\lambda > 1$. For this reason we do not assign a formal significance¹², but it can be conservatively estimated to be at least smaller than 10^{-5} . These numbers can be compared to [66], who find less strict bounds both from their CMB data (possibly since they use older Planck 2015 data). The bounds when including supernovae are remarkably similar (they find $\lambda < 0.64$ at 95% CL), but for the conversion into probability they find $1.7 \cdot 10^{-4}$ while we find a result smaller than 10^{-5} . This could be very well caused by the stronger constraint of the newer Planck data on such models in the high- λ tail of the distribution.

To check how much this is impacted by using newer BAO and SN data, we show in Fig. 4 a comparison of the older and newer data. Surprisingly, the newer data has looser bounds on the λ parameter. While at first very puzzling, this does make sense. The newer PantheonPLUS data in particular prefers relatively high values of Ω_m compared to the older data, resulting in a lower abundance of the dark energy component, which is then less restricted in λ due to its lower abundance. We summarize these constraints also in Table 2.

¹²The MCMC chains based on the Metropolis-Hastings algorithm are not necessarily incredibly well converged at this $4\text{-}5\sigma$ deviation level, and a huge number of samples would be required to make a more quantitative statement.

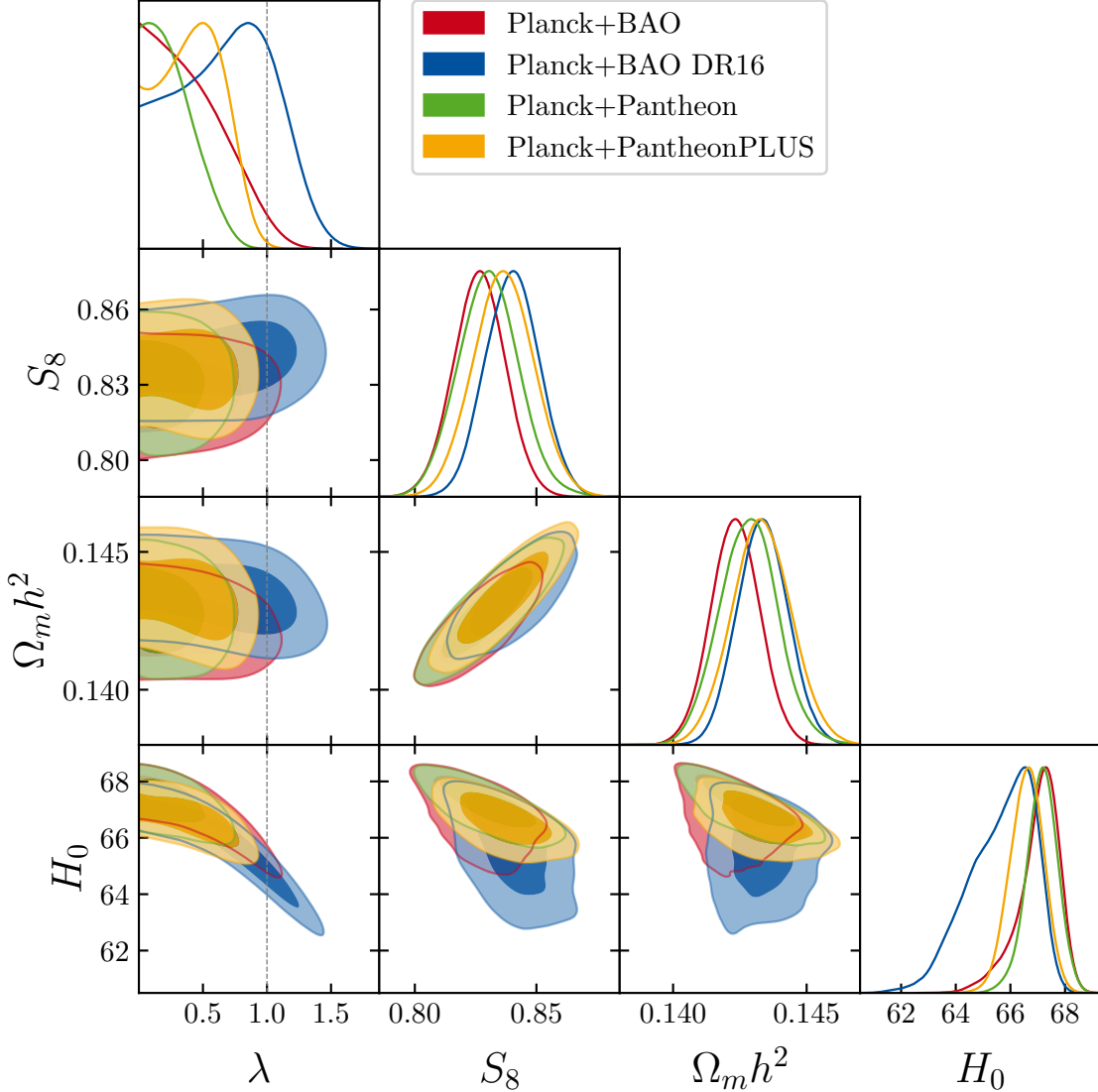


Figure 4. Comparison of the constraints on the exponential model compared between older and newer late-time cosmological data (BAO and SN).

When applying our dataset \mathcal{A} (involving Planck, BAO, Pantheon, CC, ACT, and SPT data), we find that the results are fairly similar, see Fig. 5 (indicating that BAO and supernovae data are dominating the constraining power). Here too the old data is more restrictive and has tighter constraints. We observe that in almost all cases λ and H_0 are anti-correlated, since a lower H_0 generally corresponds to a higher matter fraction Ω_m due to the tight constraint on $\Omega_m h^3$ from the Planck satellite measurement of the sound horizon angular scale. In turn, the higher matter fraction corresponds to a lower abundance of the coupled quintessence field ($\Omega_\phi \approx 1 - \Omega_m$) allowing for larger values of λ to be viable. As such, we also show how the constraints change when including a prior on H_0 from [121]. In this case, we find that the constraints on λ are a lot tighter, which given the above discussion is not entirely surprising. However, given the high tension between H_0 derived from CMB data and from the local-distance-ladder, this result should be taken with a grain of salt. We summarize the results in Table 3.

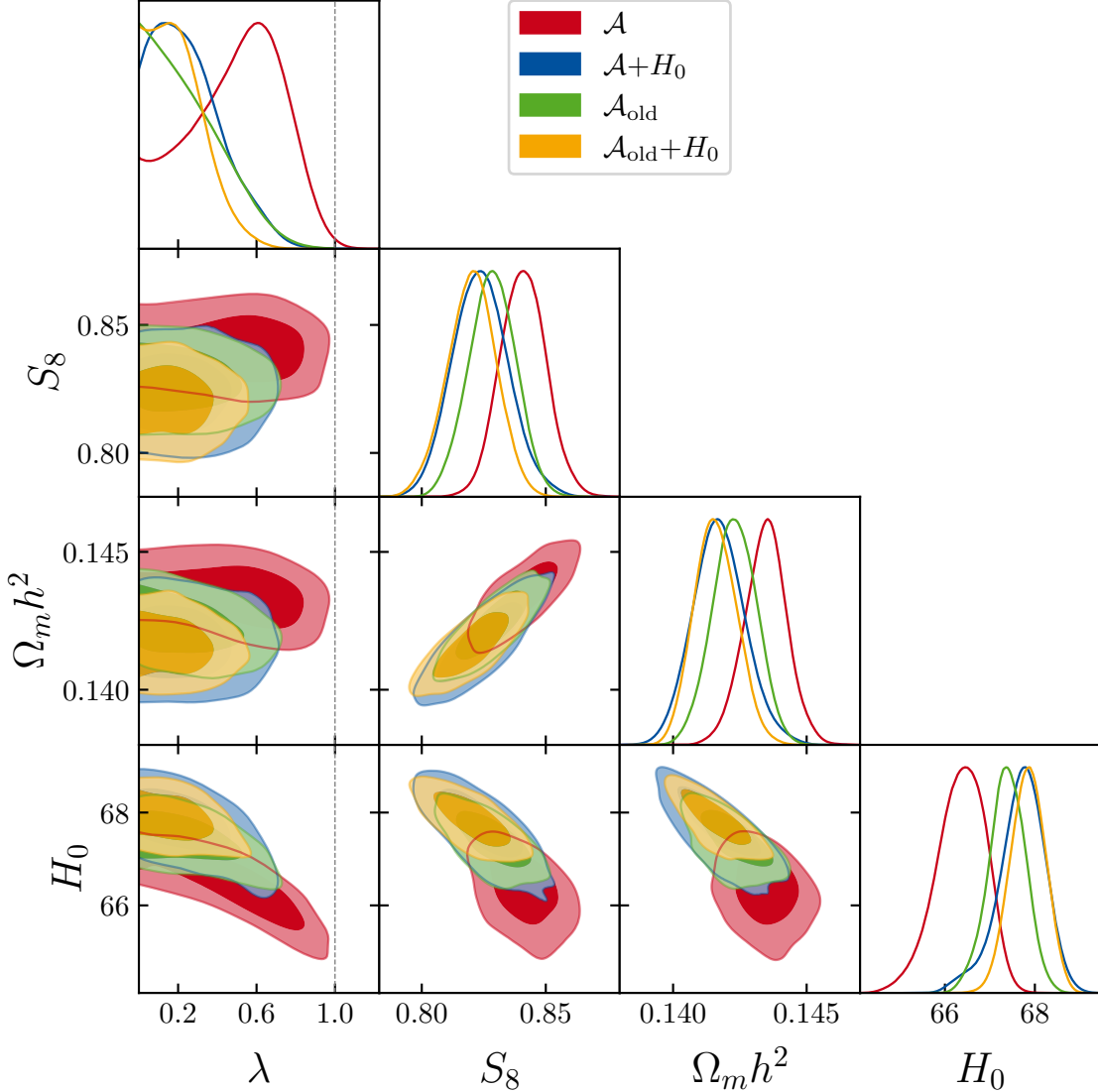


Figure 5. Comparison of the constraints on the exponential model for a variety of all data.

4.1.2 Cosine potential

Another potential with a constant Swampland criterion is given by a cosine, where the second Swampland criterion is set to some constant ($g(z) = c^2$), resulting in a potential of the type

$$V(\phi) = A \cos(c\phi/M_{\text{Pl}}) . \quad (4.3)$$

This case is also sensitive to the initial value of ϕ , since there is no scaling symmetry here, and as such we also vary the initial value. The resulting constraints are displayed in Fig. 6.

As pointed out by [66], since this model is initially frozen by Hubble drag and only begins moving during the dark energy dominated epoch (thawing model), the same tight correlation between the (relative) slope $\lambda(z)$ and the overall displacement can be observed as in the exponential case. Indeed, this is what we show in Fig. 6, using $\lambda(z = 0)$ as a proxy for the late-time slope. However, the relation is not perfect if the overall displacement $|\Delta\phi/M_{\text{Pl}}|$ becomes large. Indeed, one can derive

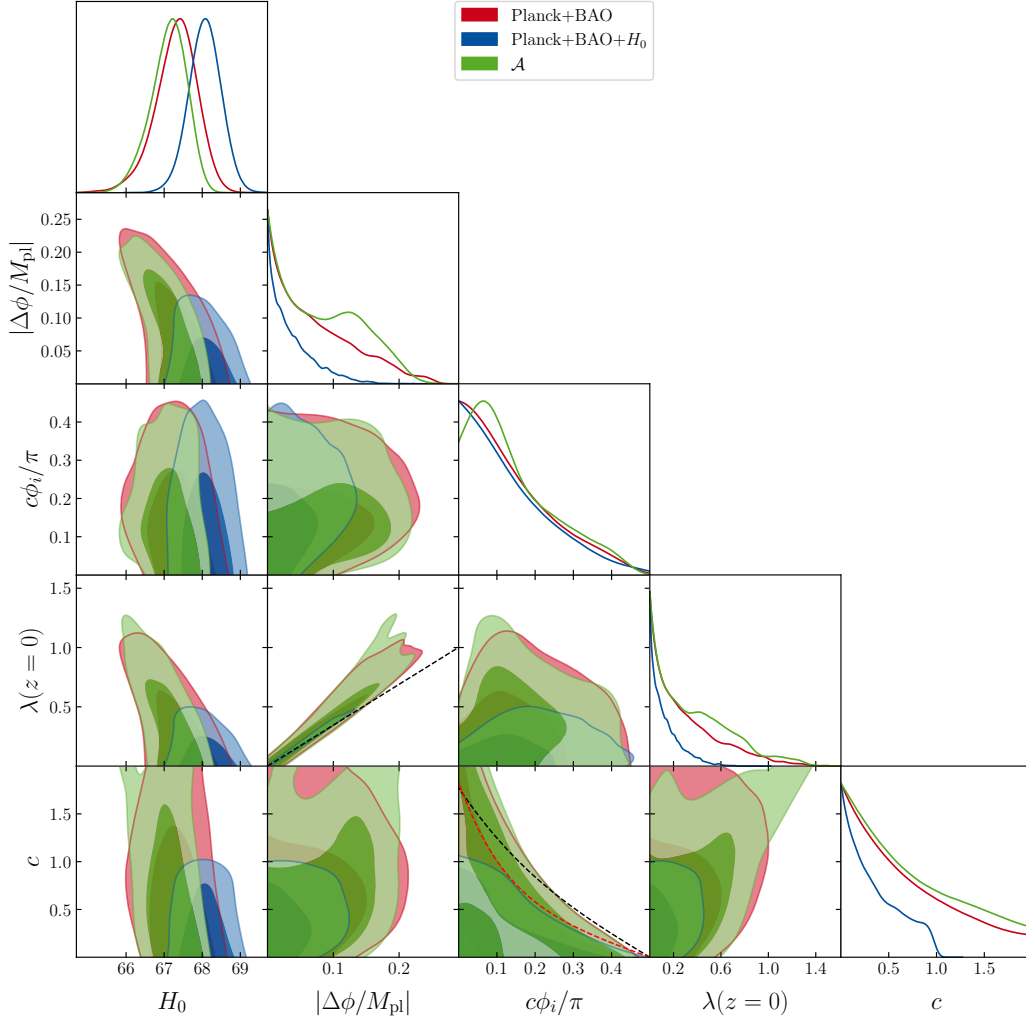


Figure 6. Constraints on the model parameters for the cosine potential model. The black dashed line in the $\lambda(z=0)$ - $|\Delta\phi/M_{Pl}|$ panel is the relation $|\Delta\phi/M_{Pl}| = 0.29\lambda(z=0)$. The black and red dashed line in the c - $c\phi_i/\pi$ panel represents Eq. (4.4) for $\lambda_{\text{eff}} = 1$ and $\lambda_{\text{eff}} = 0.5$, respectively.

using $|\Delta\phi/M_{Pl}| \simeq 0.29\lambda_{\text{eff}}$ with some effective slope λ_{eff} (note that [66] use a weighted average of $\lambda(z)$ by $\rho_\phi/\rho_{\text{crit}}$) what the relationship between the initial field ϕ_i and the cosine curvature c should be. Indeed, by definition $\lambda(z=0) = c \tan(c\phi_i/M_{Pl} + c\Delta\phi/M_{Pl})$. Approximating $\lambda(z=0)$ by λ_{eff} and using Eq. (4.2) one can find

$$\phi_i \approx -0.29\lambda_{\text{eff}} + \arctan(\lambda_{\text{eff}}/c)/c, \quad (4.4)$$

which is the curve we show in Fig. 6 for $\lambda_{\text{eff}} = 1$ (black) and $\lambda_{\text{eff}} = 0.5$ (red). As we can observe, the true constraints are deviating from this line, being especially more permissive for large values of c . Indeed, this is also noticeable in the deviation of the scaling of $|\Delta\phi/M_{Pl}|$ compared to $0.29\lambda(z=0)$. For large values of c the field traverses more different potential slopes for a given distance that it travels, breaking the tight correlations – these are not visible in [66] due to only showing the tightest dataset, which in our case would be similar to the blue contours, which do nicely follow the relation (compare for example the blue contours in the c - $c\phi_i/\pi$ panel to the red dashed line, and the tight correlation in the $|\Delta\phi/M_{Pl}|$ - $\lambda(z=0)$ panel). In this more general case we see the deviations from the simple scaling laws derived in [66] especially for large field displacements (large $|\Delta\phi/M_{Pl}|$) and

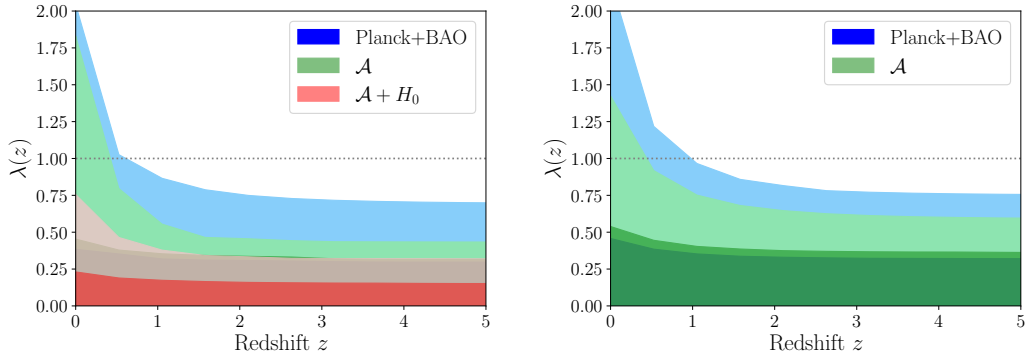


Figure 7. Constraints (68% and 95% upper limits) on $\lambda(z)$ in the cosine and axionic cosine potential. The blue contours are from Planck+BAO data, while the green contours involve the dataset \mathcal{A} . The red contours add also a H_0 prior from [121].

fast oscillations (large c). Since adding H_0 data to an otherwise incompatible (at $\sim 5\sigma$) collection of datasets is a rather questionable choice and can artificially drive constraints, we prefer to show the constraints mostly without the H_0 prior (shown in blue), and thus these deviations become important.

To summarize, the cosine potential case is very much related to the exponential case (with constant slope) especially for small c or small $\Delta\phi$ when the field cannot experience much more than the local slope during the cosmologically short dark energy domination period. The tight relations of the exponential case hold here too, except when c or $\Delta\phi$ become large. A reconstruction of the $\lambda(z)$ can be found for completeness in Fig. 7, which shows that there is a tight bound on $\lambda(z)$ during most of the history, but the $\lambda(z)$ is allowed to significantly grow towards $z \rightarrow 0$. Due to this later growth, the initial bound on λ is also tighter compared to the exponential case.

4.1.3 Axionic Cosine potential

In order to check also for more natural potentials, we investigate a toy model of the effective axionic potential (e.g. adopted in [122, 123], which is the instanton approximation¹³ [124]) as

$$V(\phi) = m^2 f^2 [1 - \cos(\phi/f)] \quad , \quad (4.5)$$

where m is an amplitude parameter and f is a frequency parameter. This model behaves very similarly to the cosine potential one (featuring also $g(z) \approx \text{const}$) since a field starting close to $\phi = f\pi - \phi_i$ will undergo a very similar evolution as one starting at $\phi = \phi_i$ in a cosine potential with $c = M_{\text{Pl}}/f$. A corresponding computation of the relation between ϕ_i and the effective slope yields

$$\pi - \phi_i \approx -0.29\lambda_{\text{eff}} + \frac{1}{c} \arctan_2 \left(\frac{-2c\lambda_{\text{eff}}}{c^2 + \lambda_{\text{eff}}^2} \middle| \frac{c^2 - \lambda_{\text{eff}}^2}{c^2 + \lambda_{\text{eff}}^2} \right) \quad (4.6)$$

where $\arctan_2(x|y) = \{\arctan(y/x) \text{ for } x > 0, \pi + \arctan(y/x) \text{ for } x < 0\}$ with $c = 1/f$, which is shown to be a good fit in Fig. 8. Given the high degree of similarity between this case and the ordinary cosine, we can draw essentially the same conclusions in this case. The only modification is a slight adjustment of where the $c - c\phi_i/\pi$ bounds occur, due to the difference between Eqs. (4.4) and (4.6). The reconstructed constraints on $\lambda(z)$ are shown in Fig. 7 and are essentially identical to those of the cosine potential. It should be noted that in this case $g(z) \neq c^2 = 1/f^2$. Indeed, a reconstruction of

¹³Looking at [124, Eq. (10)], since the up and down quarks obey $4m_u m_d / (m_u + m_d)^2 \approx 0.6$, the approximation is decent as long as m is allowed to be varied freely (giving a 3% mean square error approximation for $m \approx 1.3m_a$). As the resulting constraints are so similar to the normal cosine case, we do not expect significant changes from a more accurate modeling.

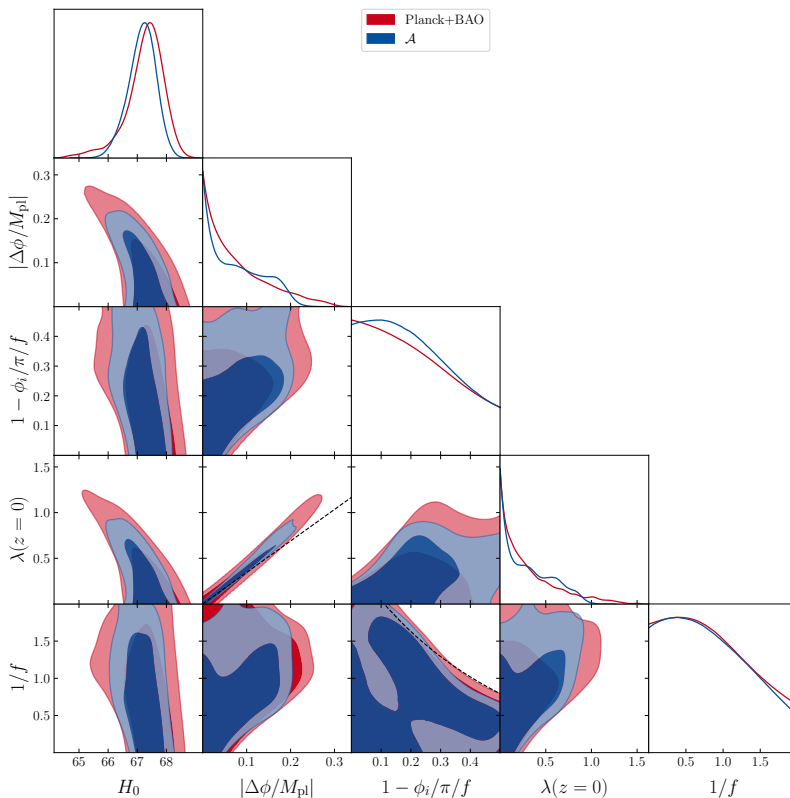


Figure 8. Same as Fig. 6 but for the axionic cosine potential of Eq. (4.5) instead.

$g(z)$ gives the approximate bound $g(z) < 1.6$ (95% CL) in this case, though it is not clear whether this is impacted by the chosen priors on $1/f$ (and as such we do not show the reconstruction).

4.1.4 Inverse exponential

This potential is defined as

$$V(\phi) = A \exp(\sigma M_{\text{Pl}}/\phi) \quad (4.7)$$

and features the possibility of the dark energy thawing into an attractor solution. We show the constraints for the parameters of this potential in Fig. 9. There is a curious bi-modality for the initial field displacement. In the low initial field displacement, the field is quickly kicked from its initial value and rolls until it overshoots the attractor solution and stops at a high displacement, before eventually rejoining the attractor solution, hence showing large displacements. On the other hand, high initial field values do not accelerate very much and are thus found with small final displacements. For the same reason higher values of σ are allowed for these fields. Overall, the correlation with the Hubble constant is mild, and the field offset is not dramatic. We also show a reconstruction of the slow roll parameters in Fig. 10. We note that as in the exponential case all curves feature $g(z) < 0$ and thus always violate the second Swampland criterion. Interestingly this model is also much more restrictive for the first Swampland criterion, $\lambda(z)$, though the constraint is very quickly deteriorating for high redshift. This is in line with the statement that the exponential case is the most conservative case for low redshift where the dark energy dominates, but also shows that the added flexibility in the inverse exponential case allows it to explore higher $\lambda(z)$ at high redshift inaccessible to many other models.

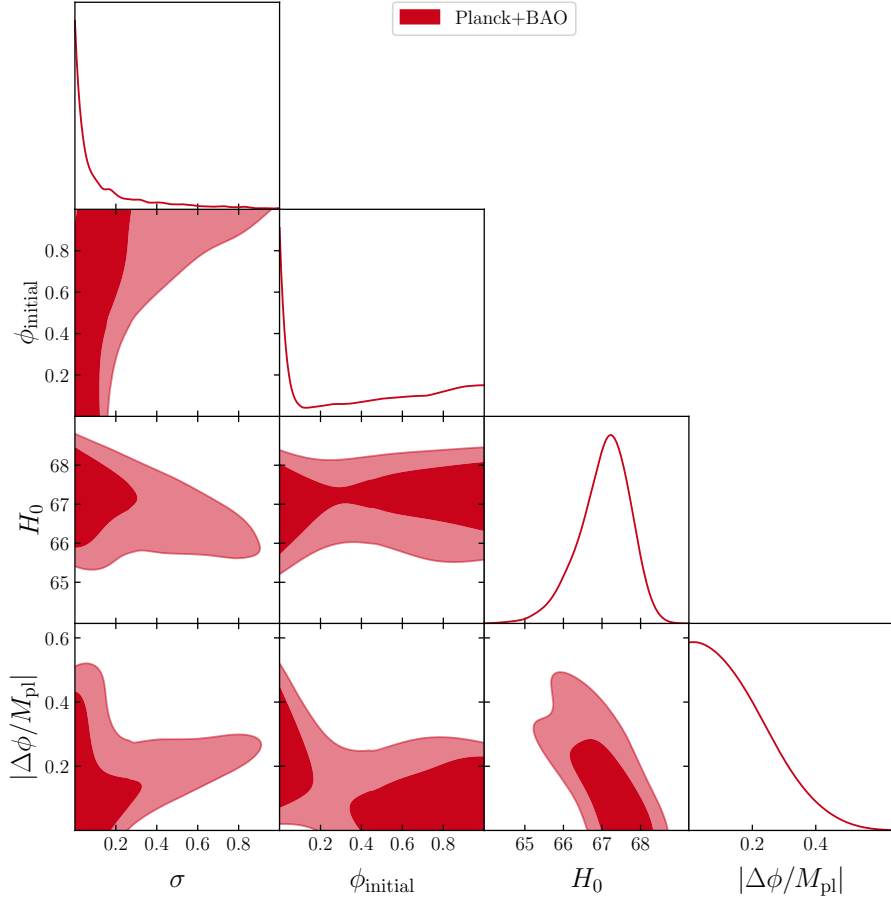


Figure 9. Constraints for the inverse exponential case.

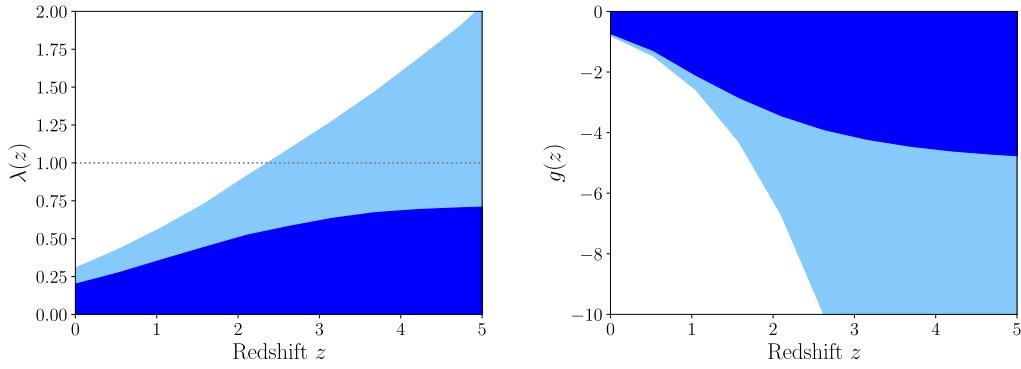


Figure 10. Reconstruction of the two Swampland criteria for the inverse exponential potential. For the first criterion we show the 1 and 2 sigma upper bound, for the second criterion we show the 1 and two sigma lower bound (since it is negative by definition, and thus the second criterion is always violated).

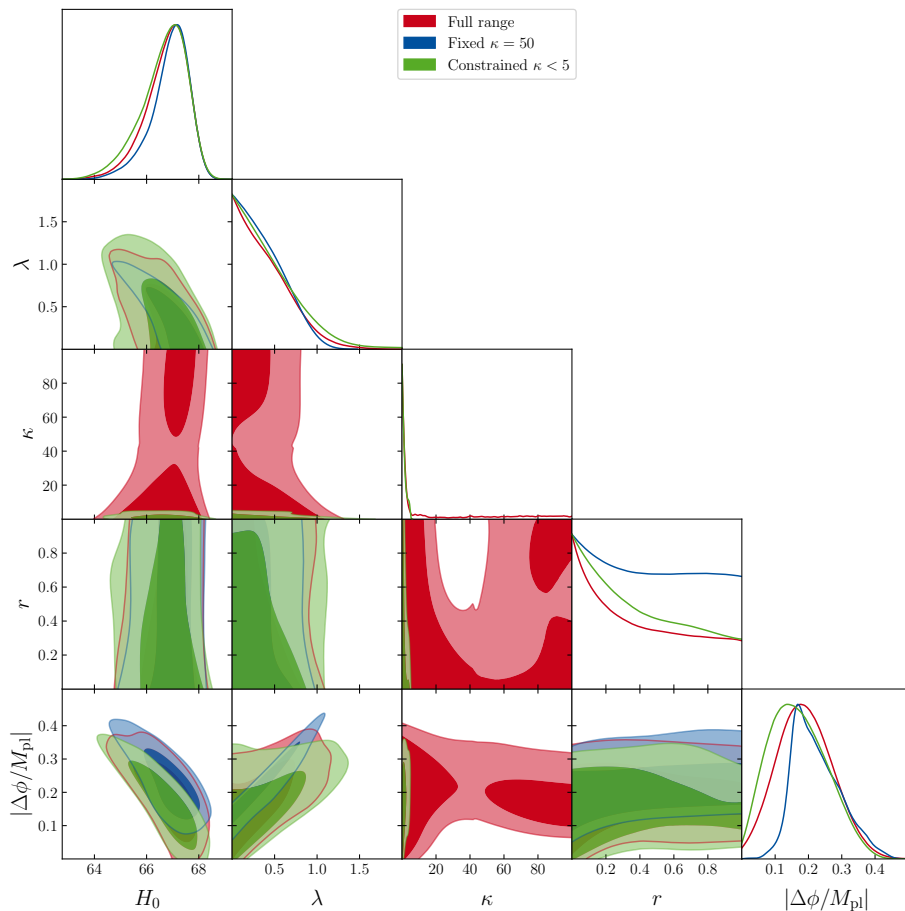


Figure 11. Constraints for the double exponential case.

4.1.5 Double exponential

The double exponential potential is defined as

$$V(\phi) = A [\exp(\lambda\phi/M_{\text{Pl}}) + r \exp(\kappa\phi/M_{\text{Pl}})] \quad (4.8)$$

where r is the ratio of the two exponential amplitudes and κ is the steepness of the second exponential. Here too a constant offset of the field $\phi \rightarrow \phi + p$ can be reabsorbed by simultaneously redefining $A \rightarrow A \exp(\lambda p/M_{\text{Pl}})$ and $r \rightarrow r \exp((\kappa - \lambda)p/M_{\text{Pl}})$, so we do not vary ϕ_i .

We show constraints for this model in Figs. 11 and 12. In a preliminary exploratory run we allow all parameters to vary in large margins, with $r \in [0, 1]$ and $\kappa \in [0, 100]$. However, the resulting parameter space is highly multi-modal. This is because the regime for large κ features one exponential that is very quickly becoming irrelevant for small displacements, leaving the other exponential to carry most of the cosmological impact. Indeed, the constraints on λ in this case are almost identical to those of the single exponential case of Section 4.1.1. Instead, the limit of small κ is also interesting where the second exponential can act in the same way as the first one, which allows the two exponentials to conspire to create more complicated potential shapes. Nevertheless we still find very competitive constraints for λ even in this case. This is because we do not allow the second potential to dominate ($r \gg 1$ is excluded by our priors), and thus the first potential will always significantly contribute to the field history, hence resulting in a tight constraint on λ throughout. It is interesting to note that around $\kappa = 50$ the tightest constraints on r are seen, and it is not quite clear why r is so constrained

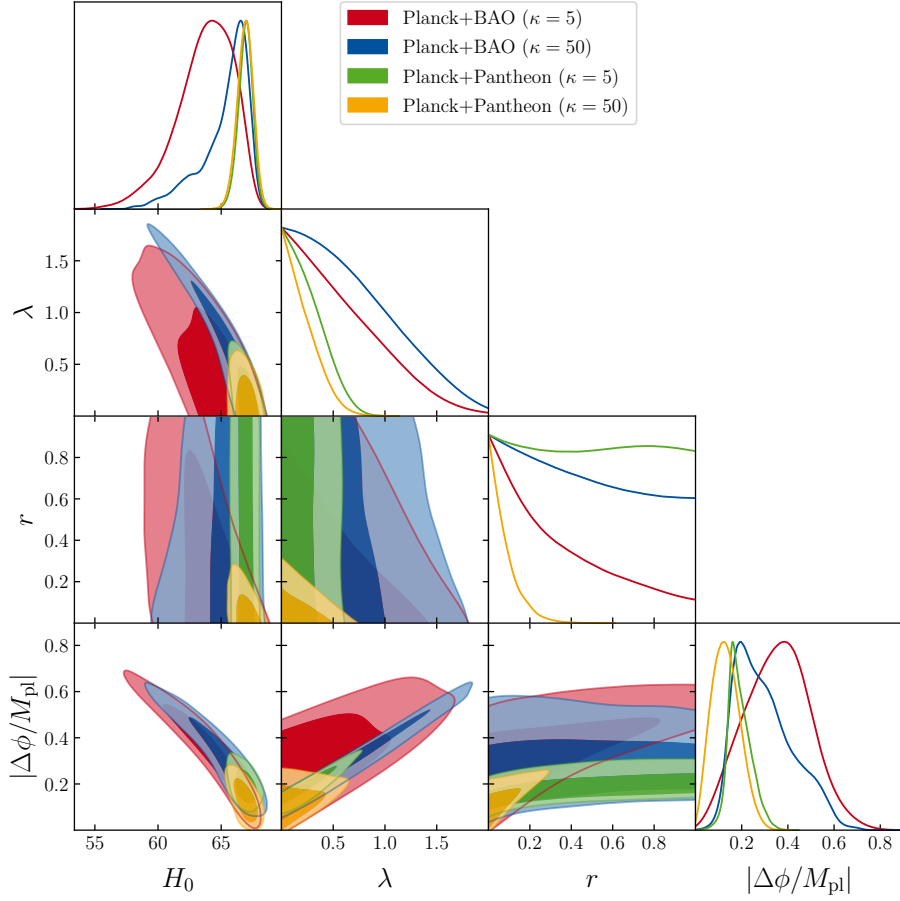


Figure 12. Constraints for the double exponential case, with either a fixed low or fixed high value of κ .

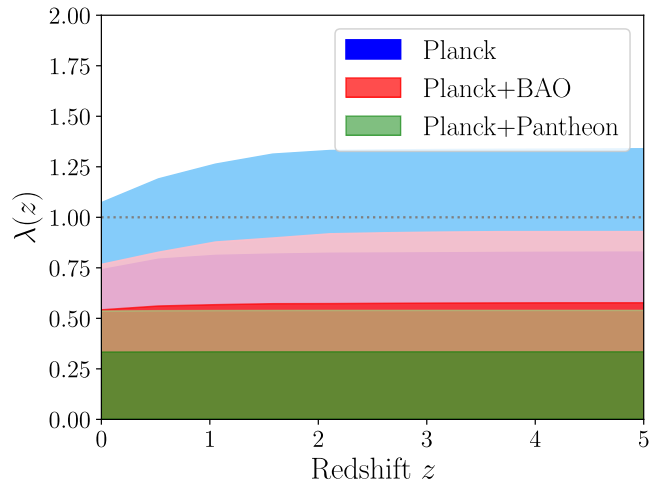


Figure 13. Low κ reconstruction of the double exponential case, clearly showing that the the effect of the second exponential is at most minute, and the constraints on λ in these cases can be seen already as sufficient.

Data combination	Constraint on $ \zeta $ (95% upper CL)
Planck+BAO	0.19
Planck+BAO+QSO+Oklo	$1.8 \cdot 10^{-5}$
Planck+BAO+QSO+Oklo+AC	$1.5 \cdot 10^{-7}$

Table 4. Constraints on the coupling parameter ζ from the various combinations of data employed within this section.

in this range. It seems that this is simply a sweet-spot where the second potential has a big impact on the overall expansion history. We separate the cases $\kappa < 5$ and $\kappa = 50$ as examples for the possible evolution of the double exponential potential, and show the constraints on these cases separately. It is interesting to note that due to the dominance of the first exponential term (since $r \in [0, 1]$) the reconstructed Swampland constraint histories are all essentially flat, as can be appreciated in Fig. 13 for a reconstruction of $\lambda(z)$ in the double exponential case with a prior on $\kappa < 5$. We essentially have $\lambda(z) \approx \lambda = \text{const}$ since the other exponential doesn't strongly contribute. This is particularly true once tighter constraints are imposed from BAO or Pantheon data.

4.2 Fine-tuning arguments

New scalar degrees of freedom have no reason a priori to be decoupled from all other fields, such as the fields underlying the standard model of particle physics. In particular, the well measured electromagnetic interaction is expected to couple with the quintessence fields if there is not some assumed fundamental reason for the coupling to be precisely zero. Given the constraints outlined below, this leaves us with two alternative problems. Either we have to construct a theoretical argument to prevent such interactions, or we have to face a great amount of fine-tuning of the interaction rate being many orders of magnitude less than what could be naturally expected. For example, one might invoke a global symmetry to suppress these couplings, but this is not a viable solution, bearing in mind that quantum gravity effects do not respect global symmetries and that there are no (unbroken) global symmetries in string theory [125]. In a nutshell, by predicting that dark energy should be dynamical (and not a cosmological constant), the Swampland criteria also predict a varying $\alpha(z)$.

The constraints on the interacting quintessence field are displayed in Fig. 14, and summarized in Table 4. While the shapes of the degeneracies are very similar with and without the fine structure data, the constraint on the coupling strengthens by multiple orders of magnitude from the observations of $\alpha(z)$. Indeed, couplings of order unity are excluded by these constraints at many thousands of σ level significance. As such, the necessary variation of $\alpha(z)$ introduced by any natural coupling would be immediately excluded by astrophysical and laboratory experiments.

The presence of a space-time variation of the fine-structure constant should also induce a violation of the universality of free-fall (for a review see [126, 127]). As such, by constraining the differential acceleration of two nearby geodesics, η , it is possible to bound the possible values for ζ [128–130]. Typically, in our case, one expects $\eta \sim O(10^{-4} - 10^{-3})\zeta^2$, such that the latest MICROSCOPE bound $\eta = (-1.5 \pm 2.7) \cdot 10^{-15}$ [131] would be less constraining than atomic clocks (as also put forward in [94] for the so-called BSBM model, and in [90] for an ultra-light scalar).¹⁴ However, the non-observation of a differential acceleration puts another independent constraint on any coupling.

In string theory, for which the Swampland conjectures are expected to be maximally motivated, such fields coupled to electromagnetism and leading to a variation of the fine structure constant are expected and unavoidable. This is the case of the moduli fields arising from compactification and more critically from the so-called dilaton field, always present along the graviton as a vibrational mode of the closed strings and setting the value of the string coupling. Several routes have been proposed to face the fine tuning issues set by measurements of the fine structure constant and tests of

¹⁴Still, the sharp MICROSCOPE bound can play a significant role in some specific varying- α models, further tightening the possible values for the coupling of the field with the rest of the standard model. For a review see [132].

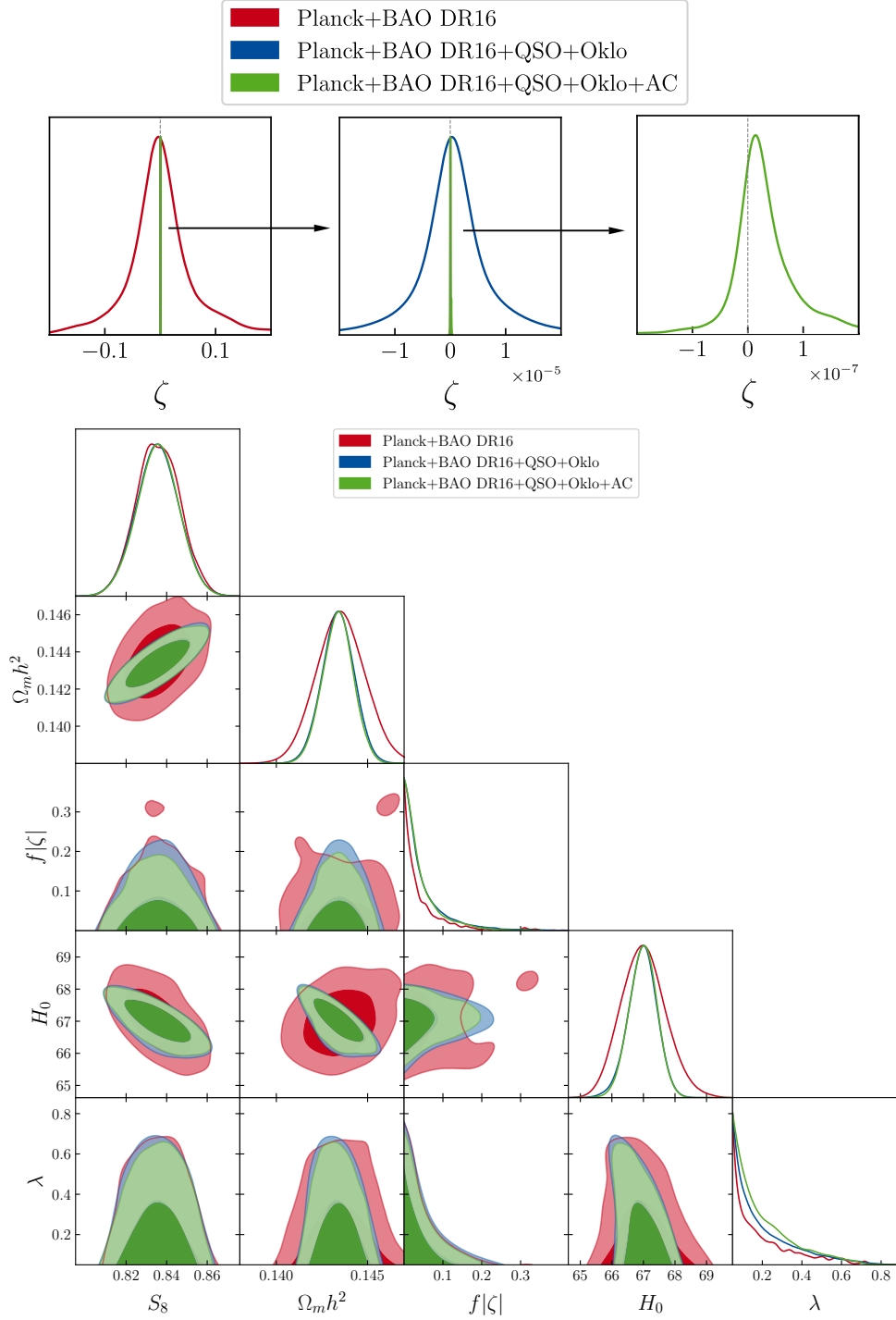


Figure 14. Constraints on ζ for the coupled and interacting coupled quintessence field. Top: Constraints on ζ alone, with a zoom-in for the $\alpha(z)$ constraints. Bottom: Full triangle plot with relevant parameters, where we transform ζ to $f|\zeta|$ with $f = 1$ for Planck+BAO DR16, $f = 10^4$ when including also QSO+Oklo data, and $f = 10^6$ when also including AC data.

the universality of free fall. For example, some “screening” mechanism could be invoked, explaining how the effects of the field could remain unnoticed in a dense environment such as the Earth (see e.g., [133]). Moreover, fields such as the dilaton could gain a significant enough mass (through e.g. supersymmetry breaking) such that their effects would be exponentially quenched with distance. [134] proposed that some attractor behavior in the matter-dilaton system could lead to the decoupling between the dilaton and the other fields of the standard model, explaining the small values of the couplings today. However, even in this situation, data drastically constrain the possible parameter space of the model, excluding most of its expected and natural values [97, 135]. On the other hand, one must also explain how to stabilize the extra compact dimensions and the associated moduli fields, in order to severely restrain their dynamics.

As such, almost any natural order coupling of the quintessence with electromagnetic fields expected from most unified theories has to face either the large hurdle of constructing a theoretical reason to effectively forbid such a coupling or has to face problems of extreme fine-tuning.

4.3 A note on model-independent reconstructions

In [76–78, 80, 81, 136] the authors put constraints on the coupled quintessence field in a model-independent way. It is important to stress that model-independence in this context does not mean independence from assumptions about the cosmological evolution. In particular, assumptions about the precise functional behavior of $H(z)$ in the quintessence model are replaced with assumptions about the smoothness of $H(z)$. However, the derived results have to be interpreted in the context of these underlying assumptions.

To outline why these assumptions are so crucial, we perform a reconstruction of expansion rate data from supernovae and cosmic chronometers below, and use this analysis to point out a few of the pitfalls of model-independent reconstructions. The first of these critical assumptions/pitfalls is the data that is used for the reconstruction. It is well known that cosmic chronometers allow for measurements of the Hubble parameter $H(z)$. However, as outlined in [112, 137] a great deal of care is to be taken, as the commonly used $H(z)$ data can be subject to biases if the systematic uncertainties (such as from the stellar population synthesis model) are not properly taken into account. For this section only, we use the data of [112] (Tab 1, which is the same as that of [138]) without any further uncertainties or correlations.

There exist little to no other cosmological data that can currently compliment these tight measurements directly. Instead, the model independent reconstructions typically fall back to the use of indirect determinations of the Hubble parameter, such as through supernovae or BAO. However, neither of these probe the Hubble expansion history directly. Without the calibration of their absolute luminosity M_B , supernovae only determine the Hubble parameter up to a multiplicative factor. Effectively, they constrain the expansion rate $E(z) = H(z)/H_0$. In order to use these data then for constraints on Swampland parameters, one has to either adopt a given value of H_0 or of M_B (which is directly equivalent to adopting a value of H_0 , since it can be converted using the same supernovae and the distance ladder approach). Similar issues arise for the use of BAO data, which measure either the angular extent of the BAO feature $\Delta\theta \propto r_s/D_A(z)$ or its redshift extent $\Delta z \propto H(z)r_s$. Typically only the latter (the parallel) measurement is used for these reconstructions. Even in this case, the measurement is not directly of $H(z)$, as crucially the sound horizon at drag r_s serves as an overall multiplicative factor. Here too some fiducial value has to be adopted in order to convert the data into $H(z)$ data. This point of requiring a fiducial model to convert $E(z)$ or $H(z)r_s$ data into $H(z)$ data is typically neglected by many reconstructions, but should be kept in mind when interpreting the results.

The data we are going to use for the reconstruction in this work are going to be the $H(z)$ and $E(z)$ data from [138] (tables 1 and 2). We also checked that the addition of BAO data from eBOSS DR16 (LRG, QSO, Lya) [104–108] does not significantly change any of the conclusions, and in order not to use any early-universe calibration (r_s) we explicitly leave out the BAO data. The data are

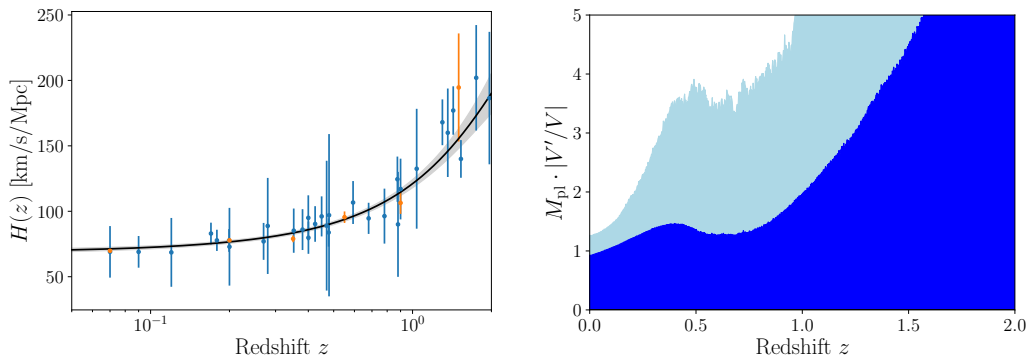


Figure 15. The reconstruction of the first Swampland criterion, using the fiducial assumptions ($H_0 = 70\text{km/s/Mpc}$, $\Omega_m = 0.3$). Left: The data used for the reconstruction, as well as the fitted Gaussian Process with a square exponential kernel (mean=black line, uncertainty=grey area). Right: The one-sided upper bounds (68%, 95%) from the quantiles of the histories, with the cuts applied on a z -dependent basis (see text). Note the similarity to the results of [76, Fig. 1] and [77, Fig. 3].

shown in Fig. 15. The first step is then to build an emulator of this $H(z)$ data with error bars. This can either be done using a Gaussian process (this work, [76, 77]), a cosmographic expansion ([79–81]), using genetic algorithms ([80]), or using other emulation techniques not adopted in these works (such as neural networks). Each of these methods uses explicitly or implicitly an assumption about the smoothness of the interpolating function. For example, cosmographic expansions and genetic algorithms typically assume infinitely differentiable basis functions. For the Gaussian Process regression, the smoothness assumption typically depends on the choice of underlying kernel function, such as the squared exponential kernel (this work), or a given order Matern kernel. This becomes important when considering that these assumptions about smoothness are fundamental when evaluating the derivative of the emulation. Indeed, the Matern- $(p + 1/2)$ kernel for the Gaussian process reconstruction only allows derivatives up to order p . Explicitly, the Matern-3/2 reconstruction would typically be subject to infinite second derivatives, and thus be entirely unable to make a statement about the Swampland conjecture. It is likely for this reason that [77] chose $p = 4$ when considering a Matern kernel (which is then already somewhat close to a squared exponential covariance function, which is the limit of the Matern kernel for $p \rightarrow \infty$). A reconstruction of the Swampland criteria without assuming a given level of smoothness is thus fundamentally impossible. In the fit with a Gaussian Process, this assumption is perhaps the most explicit, with control over the length scale as a hyperparameter that can be adapted in order to maximize the data likelihood, but in the other cases this assumption of length scales is ‘baked into’ the underlying basis functions of emulation.

Finally, in order to reconstruct $V(\phi)$ from $H(z)$ and its derivatives, one needs to explicitly subtract the non-quintessence contributions to the expansion rate. This is typically done by explicitly assuming a given value of the matter density Ω_m and declaring that apart from the quintessence at the redshifts of interest only the standard dust-like matter should be present, i.e. assuming explicitly $H^2 = M_{\text{pl}}^{-2} \rho_\phi/3 + H_0^2 \Omega_m (1+z)^3$. This, for example, explicitly neglects the impact of massive neutrinos. This is admittedly negligible for current neutrino mass bounds, but it does show that there is no complete ‘model-independence’ here. Even further, many of the analyses simply adopt a given value of Ω_m without further discussion. As we show below, the choice of Ω_m does have a non-negligible impact on the final constraints.

Even after this subtraction has been performed, there can still be problems. In particular, since now $\rho_\phi = 3M_{\text{pl}}^2 [H(z)^2 - H_0^2 \Omega_m (1+z)^3]$, there is in principle no guarantee that $\rho_\phi > 0$ for all possible emulations of $H(z)$. This means that either explicitly or implicitly part of the reconstruction space is discarded. This problem becomes even more acute when computing the kinetic term $\dot{\phi}^2 = \rho_\phi + P_\phi$ (see Eq. (2.7)), which is required to convert time-derivatives of the potential into derivatives with respect

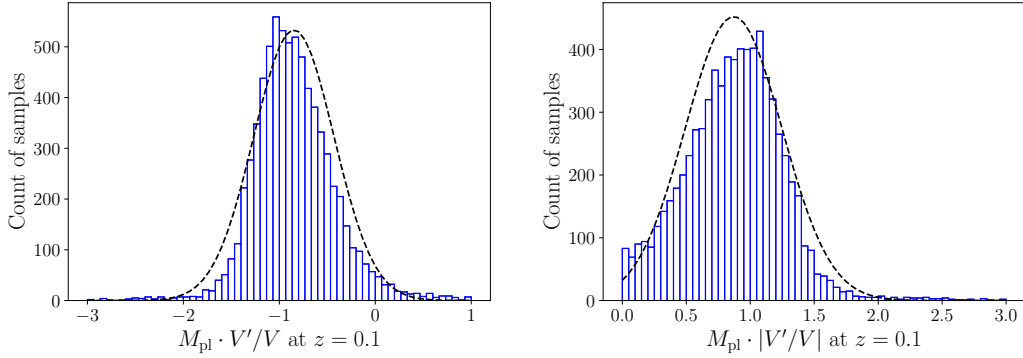


Figure 16. Distribution of samples at $z = 0.1$ for the reconstruction of V'/V and $|V'/V|$, showing that both are rather non-Gaussian distributions, especially after taking the absolute value. In blue are the histograms of the individual samples, in black are fitted Gaussian curves. We already eliminated the impact of outliers on the Gaussian fit by restricting to $V'/V \in [-3, 1]$ and $|V'/V| \in [0, 3]$.

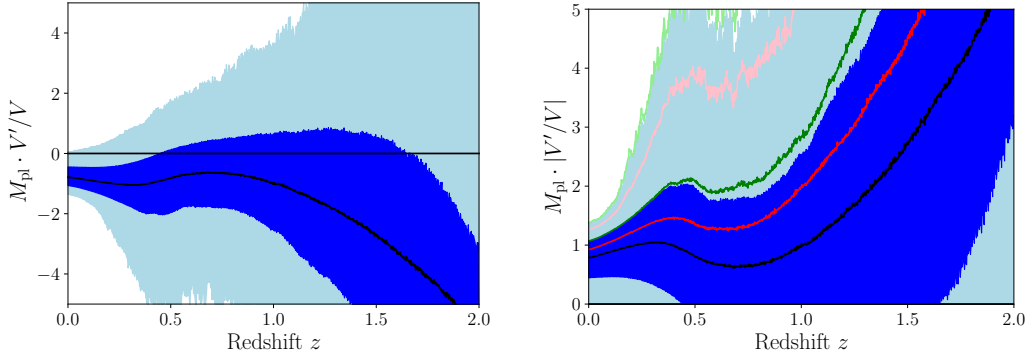


Figure 17. Comparison of techniques for deriving upper/lower quantiles on the reconstruction given a set of samples. Left: 15.87% – 84.13% quantile in dark blue, 2.275% – 97.725% quantile in light blue, and median (50% quantile) in black. Right: Different possible limits in comparison. The light-blue and dark blue contours as well as the black line are the absolute values of those from the left panel. The red and pink lines are the 68.3% and 95.4% quantiles of the absolute value samples, while the dark green and light green lines are the 84.13% and 97.725% quantiles of the absolute value samples for $|V'/V|$.

to the field. This kinetic term involves $d\rho_\phi/dz$ (or equivalently $H'(z)$) since the conservation equation implies $\dot{\rho}_\phi = -3H(\rho_\phi + P_\phi) = -3H\dot{\phi}^2$. As such, not only is $\rho_\phi > 0$ required but also $d\rho_\phi/dz > 0$. As such, for a very general emulation one naturally finds regions where these conditions are violated. In order to perform a viable analysis, either the redshift range of interest or the space of reconstructed models has to be further cut. These cuts often impose an additional prior on the corresponding model-independent bounds that is rarely explicitly discussed. If the reconstruction of V'/V , for example, is not compatible at the 1σ level with zero, this could be due to the data preferring $V'/V > 0$, or it could be a result of the various assumptions and cuts discussed above.

In our analysis, we sample¹⁵ a total of 10 000 histories from the Gaussian process that is fit to $H(z)$ and $E(z)$ data described above (the latter including the covariance), using 1000 redshift samples between 0 and 2. We impose the physicality conditions $\rho_\phi > 0$ and $d\rho_\phi/dz > 0$ discussed above for

¹⁵The results from the explicit sampling are the same as those obtained from using mean and covariance from the analytical derivatives of the Gaussian processes (when properly including also their covariance), but it gives us more flexibility about imposing cuts of physicality of $\rho_\phi > 0$ and $d\rho_\phi/dz > 0$.

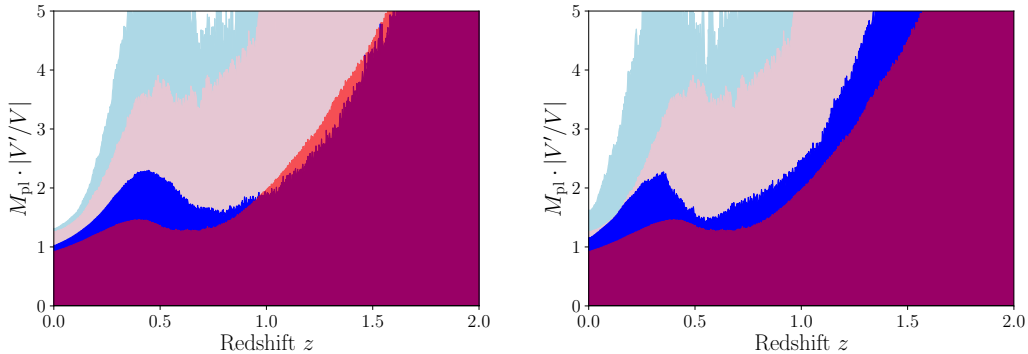


Figure 18. The reconstruction of the first Swampland criterion for a higher H_0 (up to 73km/s/Mpc) or high Ω_m (up to 0.33). The 68% and 95% upper quantile bounds are shown in dark blue and light blue, and the corresponding original bounds for comparison (from Fig. 15, right panel) are shown in slightly transparent red and pink.

each redshift independently, which in our case is a dramatic cut of around 70% of the total samples for all histories. Note that the final result does depend on how exactly such a cut is performed, as we explicitly show below.

Finally, the remaining histories can be used for bounds on $\lambda(z)$. However, one last pitfall remains when taking the absolute value of the reconstructed V'/V (which typically has large contributions from negative values). First, it is not entirely consistent to cite mean and standard deviation for $\lambda(z)$, especially after taking an absolute value. We explicitly show the non-Gaussianity in both cases in Fig. 16. Instead, one can use quantiles, though here too some care should be used. In principle, to put an upper bound on $|V'/V|$, only upper limit quantiles (such as 68% or 95%) should be used. We show the results of such an analysis in Fig. 15, which agree well with those from [76, Fig. 1] and [77, Fig. 3]. However, this is not always done, as [76, 77, 80] all use lower bounds as well. Here some careful consideration has to be made with the absolute value transformation, as otherwise interpretation is tricky. The naive lower bound of simply taking the lower quantile (e.g. 2.5% for a two-sided 2σ limit) leads to obviously wrong conclusions, since by definition it is positive definite and greater than zero even if the original function is consistent with zero at the 2σ limit. We compare in Fig. 17 different possible ways to define meaningful bounds for the absolute value. In the left panel of Fig. 17 we show the quantiles corresponding to the 1σ and 2σ limits for V'/V without absolute value, and simply transpose these into $|V'/V|$ in the right panel by taking $-V'/V$ and discarding any of the positive values (since those would give smaller bounds). As a comparison, we also display the true one-sided upper limits at the 1σ and 2σ level, which we also give in Figs. 15 and 18. Finally, we show the upper limits using the half-sided probabilities (84.13% and 97.725%) in dark and light green as well. Obviously the simplest treatment of simply cutting/transposing the graph does give decent results, though these cannot be interpreted directly as one-sided upper limits, even when the curve touches the axis. On the other hand, the one-sided limits trivially cannot show the interesting slight favor for non-zero V'/V present at $z = 0$.

Coming back to the other pitfalls, we show in Fig. 18 the dependence on the fiducial constraint on the assumed value of H_0 and Ω_m , showing that there is a rather non-negligible dependence that should be accounted for when citing any constraints. Indeed, a higher value of H_0 or Ω_m can easily weaken the constraints by more than 50% at $z \sim 0.4$.

However, by far the biggest impact is from how to treat non-physical regions. So far, we have always simply ignored the individual samples with unphysical density or field speed. However, this leads to a different number of remaining samples for each redshift. If, instead, we discard a complete history if at any redshift sample there is a negative value of ρ_ϕ or its derivative (unphysicality), we

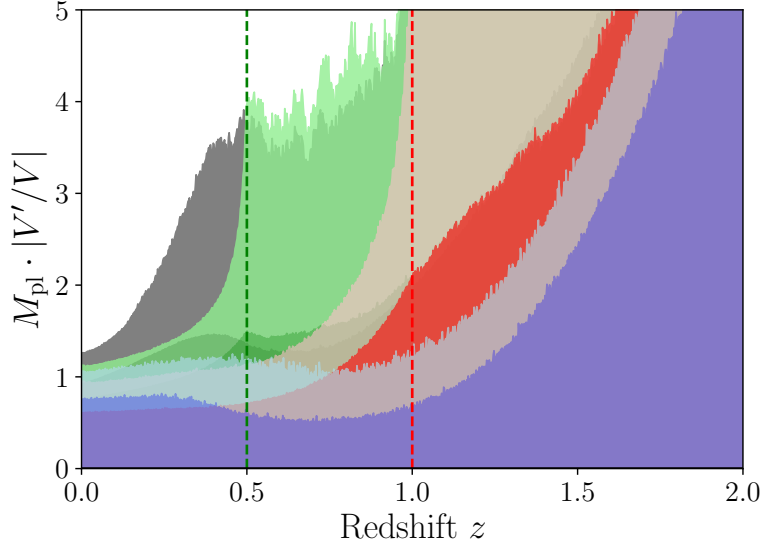


Figure 19. Different reconstructions of the first Swampland criterion with different requirements for validity (see text). The black reconstruction in the background is the one from Fig. 15 (right panel). Note the different x -axis range. The green reconstruction discards all histories, which have any non-physicality at $z < 0.5$ (green dashed line), the red reconstruction discards all histories which have any non-physicality at $z < 1$ (red dashed line), while the blue reconstruction discards all histories which have any non-physicality in the entire redshift range $z \in [0, 2]$. Note the similarity of the blue reconstruction to [80, Fig. 2] and the improved similarity of the green reconstruction to [77, Fig. 3].

instead get the constraints displayed in Fig. 19 (blue reconstruction). This reconstruction is more constraining than the original reconstruction, since histories which have larger variations of V'/V also typically feature larger H' or H'' , which gives a more varying or curved $H(z)$, and thus a higher probability for that history to also include regions of unphysicality. In Fig. 18 we explicitly see that the bump of less constraining power at $z \sim 0.4$ is at least partially caused by the varying count of the considered histories as a function of redshift, as it does not occur in any of the reconstructions which discard samples if there is an unphysicality at any redshift for the given history. We also show how the reconstruction changes by changing the redshift range over which this condition of physicality is imposed. Importantly, it remains to be stressed that even the reconstruction that discards any unphysical histories for redshift range $[0, 2]$ could be made even more stringent by considering an even broader redshift range over which to require physicality. However, since the data only reach up until $z \simeq 2$, we decided not to push the requirement of physicality further.

In summary, there are many pitfalls to the model-independent reconstruction, and the analysis is certainly not without caveats. The limits of any such analysis should be considered only in the context of these analysis choices, as otherwise conclusions are possibly severely biased, as we have shown in this section. These pitfalls include (non-exhaustive list):

- A possibly naive treatment of cosmic chronometer data systematics
- Rescaling of supernovae or BAO data using some fiducial cosmology
- Requirement to take two or three derivatives, with assumptions about functional smoothness
- Using a fiducial model for the other components (e.g. CDM+baryons)
- Regions of non-physicality have to be explicitly removed
- Taking the absolute value and how corresponding bounds are derived

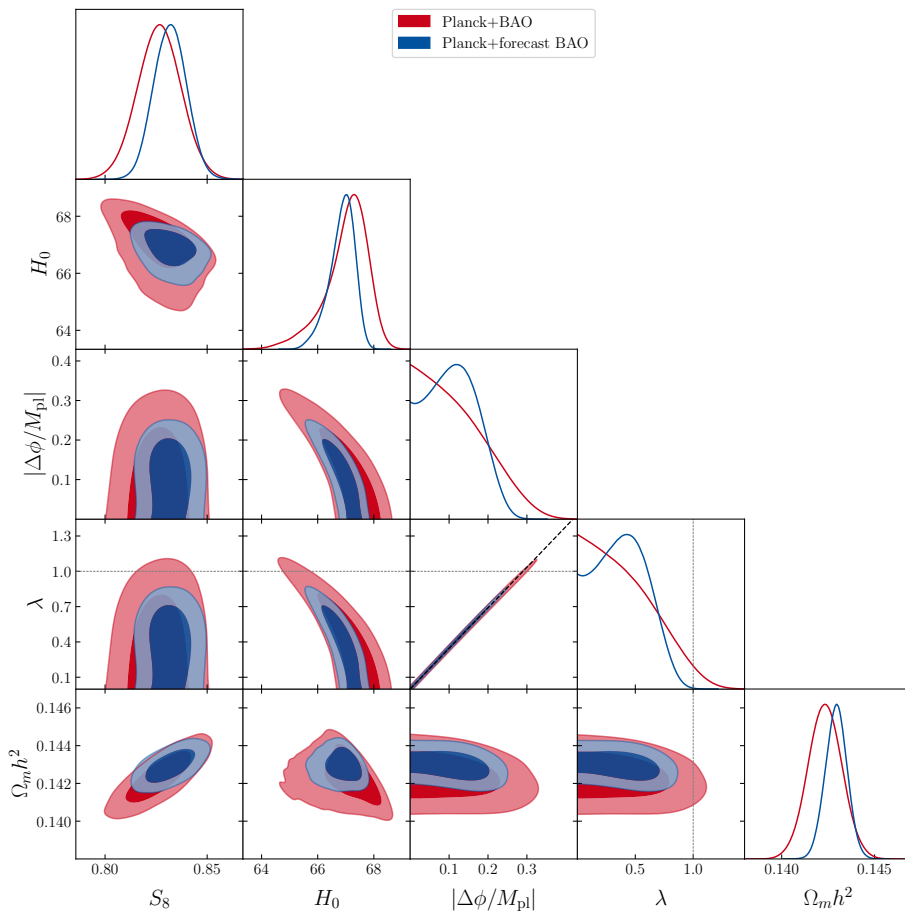


Figure 20. Same as Fig. 3, but instead adding forecasts for DESI.

4.4 Forecast constraints

We also show the forecast constraints on the exponential case of Section 4.1.1 from early forecasts of the DESI experiment error bars from [139, Sec. 2.4.3], where we use the slightly optimistic 14 000 deg² assumptions, including the use of Lyman- α data (Tab. 2.3 and 2.7). A more detailed analysis using more realistic DESI early data releases is outside the scope of this work. The resulting constraints are shown in Fig. 20. There is mild improvement on the constraining power of λ visible, with constraints improving from $\lambda < 0.94$ to $\lambda < 0.75$ at 95% CL, with the corresponding probabilities to exceed unity decreasing from 2.9% to $\sim 7 \cdot 10^{-5}$. This 25% improvement of the constraint would make this the most precise measurement of λ to date (apart from artificial choices, such as using old Pantheon data or imposing a prior on H_0 , which is incompatible with the other datasets such as Planck).

5 Conclusions

We have summarized and presented the current status of the Swampland conjectures in terms of their impact on late-time cosmology. Already from analytical arguments it is clear that there must be some mild degree of tension between the de Sitter conjectures requiring large potential slopes or curvatures and the fact that the universe is observed to undergo an accelerated expansion. We confirm this argument with current data, showing that indeed in most viable quintessence models of dark energy

these conjectures are at a mild level of tension. However, surprisingly we find that this tension did not strongly increase when adding newer BAO and Pantheon data, instead even decreasing. We argued that this is a consequence of the slightly lower dark energy abundance preferred by these probes, which allows for more flexibility in its precise evolution. In the exponential potential case, we find similar constraints to previous works [66], leading to a constraint of $\lambda = M_{\text{Pl}}|V'/V| < 0.85$ (95% CL) when using all currently available data, and $\lambda < 0.60$ (95% CL) when adding a prior on H_0 from [121], though this addition of a prior in high tension with the other datasets should be taken with a grain of salt. When instead using older BAO and supernovae data, this bound can in principle be increased up to $\lambda < 0.46$ (95% CL). We generally find that in potentials where $\lambda(z)$ is not constant that the constraints are tighter at low redshift $z \lesssim 2$, while being slightly more permissive at high redshift where the dark energy becomes irrelevant. With a view towards the second de Sitter criterion on $g(z) = -M_{\text{Pl}}^2 V''/V$, we find that the cosine potential provides similar constraints on $\lambda(z)$, though large values of $g(z)$ are still allowed in a part of the parameter space. Overall, in all cases of specific potentials we investigated, we find that there is a mild tension on the de Sitter Swampland criterion, while the distance criterion (requiring no trans-Planckian field excursions) is typically well fulfilled in all cases. However, the data is not yet precise enough to exclude order-unity slopes or large values of the second Swampland criterion.

We also outlined that there is a high degree of fine-tuning necessary to keep the coupling between the quintessence field and the electromagnetic sector tiny (or one has to invoke some deeper theoretical argument that prevents such interactions). Indeed, with the newest atomic clock likelihoods we find a constraint on the interaction as $|\zeta| < 1.5 \cdot 10^{-7}$ (95% CL), which very strongly excludes any kind of ‘natural’ $\mathcal{O}(0.1 - 10)$ coupling. As such, this fine-tuning argument presents a rather steep theoretical hurdle for consistent unified theories.

Finally, we argue that model-independent reconstructions of the Swampland criteria that have been frequently presented in the literature are subject to some pitfalls that need to be avoided for proper conclusions from the given analysis. We also argue that two of these pitfalls in particular dominate the overall conclusions from such an analysis. First, the given emulation of the expansion history has to be performed with a given modeling of the smoothness of said history, as otherwise the required derivatives cannot be taken. Second, the enforcement of a physically positive kinetic term and positive field energy density are non-trivial, and depending on the adopted method the results can change quite drastically. Together these problems imply that one can only draw conclusions from the model-independent reconstruction in the context of these major assumptions, and different assumptions can lead to different conclusions.

Overall, we find that current data are only in a relatively mild tension with the Swampland criteria, still giving string theorists large room for model building. This picture could change, however, with future data that will constrain the expansion history to an ever-increasing degree of precision. In particular, we show that forecasted constraints from DESI [139] would allow for constraints of $\lambda < 0.75$ in the late universe (already improving over the combination of all currently available data, except for the incompatible H_0 prior). As such, it might be only a matter of time until the de-Sitter Swampland criteria become incompatible with cosmological observations.

Acknowledgements

N. S. acknowledges support from the Maria de Maetzu fellowship grant: CEX2019-000918-M, financiado por MCIN/AEI/10.13039/501100011033. This work was financed by Portuguese funds through FCT - Fundação para a Ciência e a Tecnologia in the framework of the project 2022.04048.PTDC. JDFD is supported by an FCT fellowship, grant number SFRH/BD/150990/2021. CJM also acknowledges FCT and POCH/FSE (EC) support through the grant titled Investigador FCT Contract 2021.01214.CEECIND/CP1658/CT0001.

References

- [1] J. Halverson, C. Long and B. Sung, *Algorithmic universality in F-theory compactifications*, *Phys. Rev. D.* **96** (2017) 126006 [[1706.02299](#)].
- [2] C. Vafa, *The String Landscape and the Swampland*, *arXiv e-prints* (2005) hep [[hep-th/0509212](#)].
- [3] M. Brinkmann, *Challenging swampland conjectures in exotic corners of the landscape*, Ph.D. thesis, Munich U., Munich U., 2021. 10.5282/edoc.28663.
- [4] E. Palti, *The Swampland: Introduction and Review*, *Fortschritte der Physik* **67** (2019) 1900037 [[1903.06239](#)].
- [5] M. van Beest, J. Calderón-Infante, D. Mirfendereski and I. Valenzuela, *Lectures on the Swampland Program in String Compactifications*, *Phys. Rept.* **989** (2022) 1 [[2102.01111](#)].
- [6] Y. Akrami, R. Kallosh, A. Linde and V. Vardanyan, *The Landscape, the Swampland and the Era of Precision Cosmology*, *Fortsch. Phys.* **67** (2019) 1800075 [[1808.09440](#)].
- [7] K. Dasgupta, M. Emelin, E. McDonough and R. Tatar, *Quantum Corrections and the de Sitter Swampland Conjecture*, *JHEP* **01** (2019) 145 [[1808.07498](#)].
- [8] R. Kallosh, A. Linde, E. McDonough and M. Scalisi, *dS Vacua and the Swampland*, *JHEP* **03** (2019) 134 [[1901.02022](#)].
- [9] R. Blumenhagen, D. Kläwer and L. Schlechter, *Swampland Variations on a Theme by KKLt*, *JHEP* **05** (2019) 152 [[1902.07724](#)].
- [10] R. Blumenhagen, M. Brinkmann and A. Makridou, *A Note on the dS Swampland Conjecture, Non-BPS Branes and K-Theory*, *Fortsch. Phys.* **67** (2019) 1900068 [[1906.06078](#)].
- [11] S. Banerjee, U. Danielsson and S. Giri, *Curing with Hemlock: Escaping the swampland using instabilities from string theory*, *Int. J. Mod. Phys. D* **30** (2021) 2142029 [[2103.17121](#)].
- [12] P. Agrawal, G. Obied, P.J. Steinhardt and C. Vafa, *On the cosmological implications of the string Swampland*, *Physics Letters B* **784** (2018) 271 [[1806.09718](#)].
- [13] M. Scalisi and I. Valenzuela, *Swampland distance conjecture, inflation and α -attractors*, *JHEP* **08** (2019) 160 [[1812.07558](#)].
- [14] R. Blumenhagen, *Large Field Inflation/Quintessence and the Refined Swampland Distance Conjecture*, *arXiv e-prints* (2018) arXiv:1804.10504 [[1804.10504](#)].
- [15] M. Scalisi, *Inflation, Higher Spins and the Swampland*, *Phys. Lett. B* **808** (2020) 135683 [[1912.04283](#)].
- [16] H. Fukuda, R. Saito, S. Shirai and M. Yamazaki, *Phenomenological consequences of the refined swampland conjecture*, *Phys. Rev. D.* **99** (2019) 083520 [[1810.06532](#)].
- [17] S. Noori Gashti and J. Sadeghi, *Inflation, swampland and landscape*, *International Journal of Modern Physics A* **37** (2022) 2250006 [[2112.04196](#)].
- [18] J. Freigang, D. Lust, G.-E. Nian and M. Scalisi, *Cosmic Acceleration and Turns in the Swampland*, [2306.17217](#).
- [19] A. Achúcarro and G.A. Palma, *The string swampland constraints require multi-field inflation*, *J. Cosmology Astropart. Phys.* **2019** (2019) 041 [[1807.04390](#)].
- [20] S.K. Garg and C. Krishnan, *Bounds on slow roll and the de Sitter Swampland*, *Journal of High Energy Physics* **2019** (2019) 75 [[1807.05193](#)].
- [21] D. Andriot, *New Constraints on Classical de Sitter: Flirting with the Swampland*, *Fortschritte der Physik* **67** (2019) 1800103 [[1807.09698](#)].
- [22] I. Ben-Dayan, *Draining the swampland*, *Phys. Rev. D.* **99** (2019) 101301 [[1808.01615](#)].
- [23] R. Bravo, G.A. Palma and S. Riquelme, *A tip for landscape riders: multi-field inflation can fulfill the swampland distance conjecture*, *J. Cosmology Astropart. Phys.* **2020** (2020) 004 [[1906.05772](#)].
- [24] O. Bertolami and P.M. Sá, *Multi-field cold and warm inflation and the de Sitter swampland conjectures*, *J. Cosmology Astropart. Phys.* **2022** (2022) 001 [[2204.13794](#)].

- [25] S. Das, *Note on single-field inflation and the swampland criteria*, *Phys. Rev. D.* **99** (2019) 083510 [[1809.03962](#)].
- [26] C. Gungor and K.Y. Eksi, *Analytical Representation for Equations of State of Dense Matter*, *arXiv e-prints* (2011) [arXiv:1108.2166](#) [[1108.2166](#)].
- [27] V. Kamali, M. Motaharfar and R.O. Ramos, *Warm brane inflation with an exponential potential: A consistent realization away from the swampland*, *Phys. Rev. D.* **101** (2020) 023535 [[1910.06796](#)].
- [28] S. Das, G. Goswami and C. Krishnan, *Swampland, axions, and minimal warm inflation*, *Phys. Rev. D.* **101** (2020) 103529 [[1911.00323](#)].
- [29] A. Mohammadi, T. Golanbari, H. Sheikhahmadi, K. Sayar, L. Akhtari, M.A. Rasheed et al., *Warm tachyon inflation and swampland criteria*, *Chinese Physics C* **44** (2020) 095101 [[2001.10042](#)].
- [30] R. Brandenberger, V. Kamali and R.O. Ramos, *Strengthening the de Sitter swampland conjecture in warm inflation*, *Journal of High Energy Physics* **2020** (2020) 127 [[2002.04925](#)].
- [31] O. Trivedi, *Rejuvenating the hope of a swampland consistent inflated multiverse with tachyonic inflation in the high-energy RS-II braneworld*, *Modern Physics Letters A* **37** (2022) 2250162 [[2101.00638](#)].
- [32] F.B.M. dos Santos, R. Silva, S. Santos da Costa, M. Benetti and J.S. Alcaniz, *Warm β -exponential inflation and the Swampland Conjectures*, *arXiv e-prints* (2022) [arXiv:2209.06153](#) [[2209.06153](#)].
- [33] H. Matsui and F. Takahashi, *Eternal inflation and swampland conjectures*, *Phys. Rev. D.* **99** (2019) 023533 [[1807.11938](#)].
- [34] Z. Wang, R. Brandenberger and L. Heisenberg, *Eternal inflation, entropy bounds and the swampland*, *European Physical Journal C* **80** (2020) 864 [[1907.08943](#)].
- [35] W.H. Kinney, *Eternal Inflation and the Refined Swampland Conjecture*, *Physical Review Letters* **122** (2019) 081302 [[1811.11698](#)].
- [36] C.-M. Lin, *Topological eternal hilltop inflation and the swampland criteria*, *J. Cosmology Astropart. Phys.* **2020** (2020) 015 [[1912.00749](#)].
- [37] C. Osses, N. Videla and G. Panotopoulos, *Reheating in small-field inflation on the brane: the swampland criteria and observational constraints in light of the PLANCK 2018 results*, *European Physical Journal C* **81** (2021) 485 [[2101.08882](#)].
- [38] W.H. Kinney, S. Vagnozzi and L. Visinelli, *The zoo plot meets the swampland: mutual (in)consistency of single-field inflation, string conjectures, and cosmological data*, *Classical and Quantum Gravity* **36** (2019) 117001 [[1808.06424](#)].
- [39] R. Holman and B. Richard, *Spinodal solution to swampland inflationary constraints*, *Phys. Rev. D.* **99** (2019) 103508 [[1811.06021](#)].
- [40] T. Bjorkmo and M.C.D. Marsh, *Hyperinflation generalised: from its attractor mechanism to its tension with the ‘swampland conditions’*, *Journal of High Energy Physics* **2019** (2019) 172 [[1901.08603](#)].
- [41] H. Geng, *A potential mechanism for inflation from swampland conjectures*, *Physics Letters B* **805** (2020) 135430 [[1910.14047](#)].
- [42] R. Adhikari, M.R. Gangopadhyay and Yogesh, *Power law plateau inflation potential in the RS II braneworld evading swampland conjecture*, *European Physical Journal C* **80** (2020) 899 [[2002.07061](#)].
- [43] S.D. Storm and R.J. Scherrer, *Swampland conjectures and slow-roll thawing quintessence*, *Phys. Rev. D.* **102** (2020) 063519 [[2008.05465](#)].
- [44] L.A. Anchordoqui, I. Antoniadis, D. Lüst and J.F. Soriano, *S -dual inflation and the string swampland*, *Phys. Rev. D.* **103** (2021) 123537 [[2103.07982](#)].
- [45] M. Artymowski and I. Ben-Dayan, *$f(R)$ and Brans-Dicke theories and the Swampland*, *J. Cosmology Astropart. Phys.* **2019** (2019) 042 [[1902.02849](#)].
- [46] L. Heisenberg, M. Bartelmann, R. Brandenberger and A. Refregier, *Horndeski gravity in the swampland*, *Phys. Rev. D.* **99** (2019) 124020 [[1902.03939](#)].

- [47] M. Benetti, S. Capozziello and L.L. Graef, *Swampland conjecture in $f(R)$ gravity by the Noether symmetry approach*, *Phys. Rev. D.* **100** (2019) 084013 [[1905.05654](#)].
- [48] J. Sadeghi, E. Naghd Mezerji and S. Noori Gashti, *Logarithmic corrected $f(R)$ gravitational model and swampland conjectures*, *arXiv e-prints* (2019) arXiv:1910.11676 [[1910.11676](#)].
- [49] V.K. Oikonomou, I. Giannakoudi, A. Gitsis and K.-R. Revis, *Rescaled Einstein-Hilbert gravity: Inflation and the Swampland criteria*, *International Journal of Modern Physics D* **31** (2022) 2250001 [[2105.11935](#)].
- [50] J. Sadeghi, B. Pourhassan, S. Noori Gashti and S. Upadhyay, *Swampland conjecture and inflation model from brane perspective*, *Physica Scripta* **96** (2021) 125317 [[2111.15477](#)].
- [51] S. Noori Gashti, J. Sadeghi and M.R. Alipour, *Further Refining Swampland dS Conjecture in Mimetic $f(G)$ Gravity*, *Int. J. Mod. Phys. D* **32** (2022) 03 [[2212.08003](#)].
- [52] J. Sadeghi, B. Pourhassan, S. Noori Gashti, E. Naghd Mezerji and A. Pasqua, *Cosmic Evolution of the Logarithmic $f(R)$ Model and the dS Swampland Conjecture*, *Universe* **8** (2022) 623 [[2108.01448](#)].
- [53] J. Sadeghi, S. Noori Gashti and F. Darabi, *Swampland conjectures in hybrid metric-Palatini gravity*, *Phys. Dark Univ.* **37** (2022) 101090 [[2207.09793](#)].
- [54] S.N. Gashti, J. Sadeghi and B. Pourhassan, *Pleasant behavior of swampland conjectures in the face of specific inflationary models*, *Astropart. Phys.* **139** (2022) 102703 [[2202.06381](#)].
- [55] S. Brahma and M.W. Hossain, *Avoiding the string swampland in single-field inflation: excited initial states*, *Journal of High Energy Physics* **2019** (2019) 6 [[1809.01277](#)].
- [56] A. Ashoorioon, *Rescuing single field inflation from the swampland*, *Physics Letters B* **790** (2019) 568 [[1810.04001](#)].
- [57] O. Trivedi, *Lorentz violating inflation and the swampland*, *European Physical Journal Plus* **137** (2022) 507 [[2106.03578](#)].
- [58] S. Brahma, R. Brandenberger and D.-h. Yeom, *Swampland, trans-Planckian censorship and fine-tuning problem for inflation: tunnelling wavefunction to the rescue*, *J. Cosmology Astropart. Phys.* **2020** (2020) 037 [[2002.02941](#)].
- [59] V. Kamali, *Reheating after swampland conjecture*, *Journal of High Energy Physics* **2020** (2020) 92 [[1902.00701](#)].
- [60] S. Weinberg, *The cosmological constant problem*, *Reviews of Modern Physics* **61** (1989) 1.
- [61] G. Obied, H. Ooguri, L. Spodyneiko and C. Vafa, *De Sitter Space and the Swampland*, *arXiv e-prints* (2018) arXiv:1806.08362 [[1806.08362](#)].
- [62] R.R. Caldwell, R. Dave and P.J. Steinhardt, *Cosmological Imprint of an Energy Component with General Equation of State*, *Physical Review Letters* **80** (1998) 1582 [[astro-ph/9708069](#)].
- [63] L. Heisenberg, M. Bartelmann, R. Brandenberger and A. Refregier, *Dark energy in the swampland*, *Phys. Rev. D.* **98** (2018) 123502 [[1808.02877](#)].
- [64] L. Heisenberg, M. Bartelmann, R. Brandenberger and A. Refregier, *Dark energy in the Swampland II*, *Science China Physics, Mechanics, and Astronomy* **62** (2019) 990421 [[1809.00154](#)].
- [65] D. Wang, *Multi-feature universe: large parameter space cosmology and the swampland*, *arXiv e-prints* (2018) arXiv:1809.04854 [[1809.04854](#)].
- [66] M. Raveri, W. Hu and S. Sethi, *Swampland conjectures and late-time cosmology*, *Phys. Rev. D.* **99** (2019) 083518 [[1812.10448](#)].
- [67] E.Ó. Colgáin and H. Yavartanoo, *Testing the Swampland: H_0 tension*, *arXiv e-prints* (2019) arXiv:1905.02555 [[1905.02555](#)].
- [68] O. Trivedi, *Implications of single field inflation in general cosmological scenarios on the nature of dark energy given the swampland conjectures*, *Int. J. Geom. Meth. Mod. Phys.* **18** (2021) 2150231 [[2011.14316](#)].
- [69] R.-G. Cai, S. Khimphun, B.-H. Lee, S. Sun, G. Tumurtushaa and Y.-L. Zhang, *Emergent dark universe and the swampland criteria*, *Physics of the Dark Universe* **26** (2019) 100387 [[1812.11105](#)].

- [70] S. Brahma and M.W. Hossain, *Dark energy beyond quintessence: constraints from the swampland*, *Journal of High Energy Physics* **2019** (2019) 70 [[1902.11014](#)].
- [71] C. van de Bruck and C.C. Thomas, *Dark energy, the swampland, and the equivalence principle*, *Phys. Rev. D.* **100** (2019) 023515 [[1904.07082](#)].
- [72] U. Mukhopadhyay and D. Majumdar, *Swampland criteria in the slotheon field dark energy*, *Phys. Rev. D.* **100** (2019) 024006 [[1904.01455](#)].
- [73] L.A. Anchordoqui, I. Antoniadis, D. Lüst, J.F. Soriano and T.R. Taylor, *H_0 tension and the string swampland*, *Phys. Rev. D.* **101** (2020) 083532 [[1912.00242](#)].
- [74] G. Montefalcone, P.J. Steinhardt and D.H. Wesley, *Dark energy, extra dimensions, and the Swampland*, *Journal of High Energy Physics* **2020** (2020) 91 [[2005.01143](#)].
- [75] V.K. Oikonomou, *Rescaled Einstein-Hilbert gravity from $f(R)$ gravity: Inflation, dark energy, and the swampland criteria*, *Phys. Rev. D.* **103** (2021) 124028 [[2012.01312](#)].
- [76] T. Yang, *Model independent perspectives on coupled dark energy and the swampland*, *Phys. Rev. D.* **102** (2020) 083511 [[2006.14511](#)].
- [77] E. Elizalde and M. Khurshudyan, *Swampland criteria for a dark energy dominated universe ensuing from Gaussian processes and $H(z)$ data analysis*, *Phys. Rev. D.* **99** (2019) 103533 [[1811.03861](#)].
- [78] E. Elizalde and M. Khurshudyan, *Interplay between Swampland and Bayesian Machine Learning in constraining cosmological models*, *European Physical Journal C* **81** (2021) 335 [[2007.02369](#)].
- [79] A. Banerjee, H. Cai, L. Heisenberg, E.Ó. Colgáin, M.M. Sheikh-Jabbari and T. Yang, *Hubble sinks in the low-redshift swampland*, *Phys. Rev. D.* **103** (2021) L081305 [[2006.00244](#)].
- [80] R. Arjona and S. Nesseris, *Machine learning and cosmographic reconstructions of quintessence and the swampland conjectures*, *Phys. Rev. D.* **103** (2021) 063537 [[2012.12202](#)].
- [81] L. Heisenberg, M. Bartelmann, R. Brandenberger and A. Refregier, *Model independent analysis of supernova data, dark energy, trans-Planckian censorship and the swampland*, *Physics Letters B* **812** (2021) 135990 [[2003.13283](#)].
- [82] H. Ooguri and C. Vafa, *On the geometry of the string landscape and the swampland*, *Nuclear Physics B* **766** (2007) 21 [[hep-th/0605264](#)].
- [83] F. Baume and E. Palti, *Backreacted axion field ranges in string theory*, *Journal of High Energy Physics* **2016** (2016) 43 [[1602.06517](#)].
- [84] D. Klaewer and E. Palti, *Super-Planckian spatial field variations and quantum gravity*, *Journal of High Energy Physics* **2017** (2017) 88 [[1610.00010](#)].
- [85] R. Bousso, *A covariant entropy conjecture*, *Journal of High Energy Physics* **1999** (1999) 004 [[hep-th/9905177](#)].
- [86] J.D. Bekenstein, *Black holes and the second law.*, *Nuovo Cimento Lettere* **4** (1972) 737.
- [87] R. Bousso, *Light Sheets and Bekenstein's Entropy Bound*, *Physical Review Letters* **90** (2003) 121302 [[hep-th/0210295](#)].
- [88] H. Ooguri, E. Palti, G. Shiu and C. Vafa, *Distance and de Sitter conjectures on the Swampland*, *Physics Letters B* **788** (2019) 180 [[1810.05506](#)].
- [89] D. Andriot and C. Roupec, *Further Refining the de Sitter Swampland Conjecture*, *Fortschritte der Physik* **67** (2019) 1800105 [[1811.08889](#)].
- [90] M. Archidiacono, E. Castorina, D. Redigolo and E. Salvioni, *Unveiling dark fifth forces with linear cosmology*, *JCAP* **10** (2022) 074 [[2204.08484](#)].
- [91] S. Tsujikawa, *Quintessence: a review*, *Classical and Quantum Gravity* **30** (2013) 214003 [[1304.1961](#)].
- [92] J.D. Bekenstein, *Fine-structure constant: Is it really a constant?*, *Phys. Rev. D.* **25** (1982) 1527.
- [93] K.A. Olive and M. Pospelov, *Evolution of the fine structure constant driven by dark matter and the cosmological constant*, *Phys. Rev. D.* **65** (2002) 085044 [[hep-ph/0110377](#)].

- [94] L. Vacher, J.D.F. Dias, N. Schöneberg, C.J.A.P. Martins, S. Vinzl, S. Nesseris et al., *Constraints on extended Bekenstein models from cosmological, astrophysical, and local data*, *Phys. Rev. D.* **106** (2022) 083522 [[2207.03258](#)].
- [95] Particle Data Group, P.A. Zyla, R.M. Barnett, J. Beringer, O. Dahl, D.A. Dwyer et al., *Review of Particle Physics*, *Progress of Theoretical and Experimental Physics* **2020** (2020) 083C01.
- [96] J. Lesgourgues, *The cosmic linear anisotropy solving system (class) i: Overview*, 2011.
- [97] L. Vacher, N. Schöneberg, J.D.F. Dias, C.J.A.P. Martins and F. Pimenta, *Runaway dilaton models: Improved constraints from the full cosmological evolution*, *Phys. Rev. D.* **107** (2023) 104002 [[2301.13500](#)].
- [98] N. Lee, Y. Ali-Haïmoud, N. Schöneberg and V. Poulin, *What It Takes to Solve the Hubble Tension through Modifications of Cosmological Recombination*, *Physical Review Letters* **130** (2023) 161003 [[2212.04494](#)].
- [99] Planck Collaboration, N. Aghanim, Y. Akrami, M. Ashdown, J. Aumont, C. Baccigalupi et al., *Planck 2018 results. V. CMB power spectra and likelihoods*, *Astronomy and Astrophysics* **641** (2020) A5 [[1907.12875](#)].
- [100] Planck Collaboration, N. Aghanim, Y. Akrami, M. Ashdown, J. Aumont, C. Baccigalupi et al., *Planck 2018 results. VIII. Gravitational lensing*, *Astronomy and Astrophysics* **641** (2020) A8 [[1807.06210](#)].
- [101] F. Beutler, C. Blake, M. Colless, D.H. Jones, L. Staveley-Smith, L. Campbell et al., *The 6dF Galaxy Survey: baryon acoustic oscillations and the local Hubble constant*, *Monthly Notices of the Royal Astronomical Society* **416** (2011) 3017 [[1106.3366](#)].
- [102] A.J. Ross, L. Samushia, C. Howlett, W.J. Percival, A. Burden and M. Manera, *The clustering of the SDSS DR7 main Galaxy sample - I. A 4 per cent distance measure at $z = 0.15$* , *Monthly Notices of the Royal Astronomical Society* **449** (2015) 835 [[1409.3242](#)].
- [103] S. Alam, M. Ata, S. Bailey, F. Beutler, D. Bizyaev, J.A. Blazek et al., *The clustering of galaxies in the completed SDSS-III Baryon Oscillation Spectroscopic Survey: cosmological analysis of the DR12 galaxy sample*, *Monthly Notices of the Royal Astronomical Society* **470** (2017) 2617 [[1607.03155](#)].
- [104] S. Alam, M. Aubert, S. Avila, C. Balland, J.E. Bautista, M.A. Bershady et al., *Completed SDSS-IV extended Baryon Oscillation Spectroscopic Survey: Cosmological implications from two decades of spectroscopic surveys at the Apache Point Observatory*, *Phys. Rev. D.* **103** (2021) 083533 [[2007.08991](#)].
- [105] H. Gil-Marín, J.E. Bautista, R. Paviot, M. Vargas-Magaña, S. de la Torre, S. Fromenteau et al., *The Completed SDSS-IV extended Baryon Oscillation Spectroscopic Survey: measurement of the BAO and growth rate of structure of the luminous red galaxy sample from the anisotropic power spectrum between redshifts 0.6 and 1.0*, *Monthly Notices of the Royal Astronomical Society* **498** (2020) 2492 [[2007.08994](#)].
- [106] J.E. Bautista, R. Paviot, M. Vargas Magaña, S. de la Torre, S. Fromenteau, H. Gil-Marín et al., *The completed SDSS-IV extended Baryon Oscillation Spectroscopic Survey: measurement of the BAO and growth rate of structure of the luminous red galaxy sample from the anisotropic correlation function between redshifts 0.6 and 1*, *Monthly Notices of the Royal Astronomical Society* **500** (2021) 736 [[2007.08993](#)].
- [107] J. Hou, A.G. Sánchez, A.J. Ross, A. Smith, R. Neveux, J. Bautista et al., *The completed SDSS-IV extended Baryon Oscillation Spectroscopic Survey: BAO and RSD measurements from anisotropic clustering analysis of the quasar sample in configuration space between redshift 0.8 and 2.2*, *Monthly Notices of the Royal Astronomical Society* **500** (2021) 1201 [[2007.08998](#)].
- [108] R. Neveux, E. Burtin, A. de Mattia, A. Smith, A.J. Ross, J. Hou et al., *The completed SDSS-IV extended Baryon Oscillation Spectroscopic Survey: BAO and RSD measurements from the anisotropic power spectrum of the quasar sample between redshift 0.8 and 2.2*, *Monthly Notices of the Royal Astronomical Society* **499** (2020) 210 [[2007.08999](#)].
- [109] H. du Mas des Bourboux, J. Rich, A. Font-Ribera, V. de Sainte Agathe, J. Farr, T. Etourneau et al., *The Completed SDSS-IV Extended Baryon Oscillation Spectroscopic Survey: Baryon Acoustic Oscillations with Ly α Forests*, *The Astrophysical Journal* **901** (2020) 153 [[2007.08995](#)].

- [110] D.M. Scolnic, D.O. Jones, A. Rest, Y.C. Pan, R. Chornock, R.J. Foley et al., *The Complete Light-curve Sample of Spectroscopically Confirmed SNe Ia from Pan-STARRS1 and Cosmological Constraints from the Combined Pantheon Sample*, *The Astrophysical Journal* **859** (2018) 101 [1710.00845].
- [111] D. Scolnic, D. Brout, A. Carr, A.G. Riess, T.M. Davis, A. Dwomoh et al., *The Pantheon+ Analysis: The Full Data Set and Light-curve Release*, *The Astrophysical Journal* **938** (2022) 113 [2112.03863].
- [112] M. Moresco, L. Amati, L. Amendola, S. Birrer, J.P. Blakeslee, M. Cantiello et al., *Unveiling the Universe with emerging cosmological probes*, *Living Reviews in Relativity* **25** (2022) 6 [2201.07241].
- [113] S. Aiola, E. Calabrese, L. Maurin, S. Naess, B.L. Schmitt, M.H. Abitbol et al., *The Atacama Cosmology Telescope: DR4 maps and cosmological parameters*, *J. Cosmology Astropart. Phys.* **2020** (2020) 047 [2007.07288].
- [114] L. Balkenhol, D. Dutcher, A. Spurio Mancini, A. Doussot, K. Benabed, S. Galli et al., *Measurement of the CMB temperature power spectrum and constraints on cosmology from the SPT-3G 2018 T T , T E , and E E dataset*, *Phys. Rev. D.* **108** (2023) 023510 [2212.05642].
- [115] C.J.A.P. Martins, *The status of varying constants: a review of the physics, searches and implications*, *Reports on Progress in Physics* **80** (2017) 126902 [1709.02923].
- [116] M.T. Murphy and K.L. Cooksey, *Subaru Telescope limits on cosmological variations in the fine-structure constant*, *Monthly Notices of the Royal Astronomical Society* **471** (2017) 4930 [<https://academic.oup.com/mnras/article-pdf/471/4/4930/19650209/stx1949.pdf>].
- [117] J.K. Webb, J.A. King, M.T. Murphy, V.V. Flambaum, R.F. Carswell and M.B. Bainbridge, *Indications of a Spatial Variation of the Fine Structure Constant*, *Physical Review Letters* **107** (2011) 191101 [1008.3907].
- [118] M.T. Murphy, P. Molaro, A.C.O. Leite, G. Cupani, S. Cristiani, V. D’Odorico et al., *Fundamental physics with ESPRESSO: Precise limit on variations in the fine-structure constant towards the bright quasar HE 0515–4414*, *Astronomy and Astrophysics* **658** (2022) A123 [2112.05819].
- [119] Y.V. Petrov, A.I. Nazarov, M.S. Onegin, V.Y. Petrov and E.G. Sakhnovsky, *Natural nuclear reactor at Oklo and variation of fundamental constants: Computation of neutronics of a fresh core*, *Phys. Rev. C.* **74** (2006) 064610 [hep-ph/0506186].
- [120] M. Filzinger, S. Dörscher, R. Lange, J. Klose, M. Steinel, E. Benkler et al., *Improved limits on the coupling of ultralight bosonic dark matter to photons from optical atomic clock comparisons*, *arXiv e-prints* (2023) arXiv:2301.03433 [2301.03433].
- [121] A.G. Riess, W. Yuan, L.M. Macri, D. Scolnic, D. Brout, S. Casertano et al., *A Comprehensive Measurement of the Local Value of the Hubble Constant with $1 \text{ km s}^{-1} \text{ Mpc}^{-1}$ Uncertainty from the Hubble Space Telescope and the SH0ES Team*, *ApJ Letters* **934** (2022) L7 [2112.04510].
- [122] M. Kamionkowski, J. Pradler and D.G.E. Walker, *Dark Energy from the String Axiverse*, *Physical Review Letters* **113** (2014) 251302 [1409.0549].
- [123] V. Poulin, T.L. Smith, T. Karwal and M. Kamionkowski, *Early Dark Energy can Resolve the Hubble Tension*, *Physical Review Letters* **122** (2019) 221301 [1811.04083].
- [124] G.G. di Cortona, E. Hardy, J.P. Vega and G. Villadoro, *The QCD axion, precisely*, *Journal of High Energy Physics* **2016** (2016) 34 [1511.02867].
- [125] T. Banks and L.J. Dixon, *Constraints on String Vacua with Space-Time Supersymmetry*, *Nucl. Phys. B* **307** (1988) 93.
- [126] T. Damour, *The Equivalence Principle and the Constants of Nature*, *Space Science Review* **148** (2009) 191 [0906.3174].
- [127] J.-P. Uzan, *Varying Constants, Gravitation and Cosmology*, *Living Reviews in Relativity* **14** (2011) 2 [1009.5514].
- [128] S.M. Carroll, *Quintessence and the Rest of the World: Suppressing Long-Range Interactions*, *Physical Review Letters* **81** (1998) 3067 [astro-ph/9806099].
- [129] G. Dvali and M. Zaldarriaga, *Changing α with Time: Implications for Fifth-Force-Type Experiments and Quintessence*, *Physical Review Letters* **88** (2002) 091303 [hep-ph/0108217].

- [130] T. Chiba and K. Kohri, *Quintessence Cosmology and Varying α* , *Progress of Theoretical Physics* **107** (2002) 631 [[hep-ph/0111086](#)].
- [131] P. Touboul, G. Métris, M. Rodrigues, J. Bergé, A. Robert, Q. Baghi et al., *M I C R O S C O P E Mission: Final Results of the Test of the Equivalence Principle*, *Physical Review Letters* **129** (2022) 121102 [[2209.15487](#)].
- [132] J. Bergé, *Microscope's view at gravitation*, *Reports on Progress in Physics* **86** (2023) 066901.
- [133] L. ter Haar, M. Bezares, M. Crisostomi, E. Barausse and C. Palenzuela, *Dynamics of Screening in Modified Gravity*, *Physical Review Letters* **126** (2021) 091102 [[2009.03354](#)].
- [134] T. Damour and A.M. Polyakov, *The string dilation and a least coupling principle*, *Nuclear Physics B* **423** (1994) 532 [[hep-th/9401069](#)].
- [135] C.J.A.P. Martins and L. Vacher, *Astrophysical and local constraints on string theory: Runaway dilaton models*, *Phys. Rev. D.* **100** (2019) 123514 [[1911.10821](#)].
- [136] M. Park, M. Raveri and B. Jain, *Reconstructing quintessence*, *Phys. Rev. D.* **103** (2021) 103530 [[2101.04666](#)].
- [137] M. Moresco, R. Jimenez, L. Verde, A. Cimatti and L. Pozzetti, *Setting the Stage for Cosmic Chronometers. II. Impact of Stellar Population Synthesis Models Systematics and Full Covariance Matrix*, *The Astrophysical Journal* **898** (2020) 82 [[2003.07362](#)].
- [138] A. Gómez-Valent and L. Amendola, *H_0 from cosmic chronometers and Type Ia supernovae, with Gaussian Processes and the novel Weighted Polynomial Regression method*, *J. Cosmology Astropart. Phys.* **2018** (2018) 051 [[1802.01505](#)].
- [139] DESI Collaboration, A. Aghamousa, J. Aguilar, S. Ahlen, S. Alam, L.E. Allen et al., *The DESI Experiment Part I: Science, Targeting, and Survey Design*, *arXiv e-prints* (2016) [arXiv:1611.00036](#) [[1611.00036](#)].